Clinical Neurophysiology 121 (2010) 21–38

Contents lists available at ScienceDirect

Clinical Neurophysiology

journal homepage: www.elsevier.com/locate/clinph

Neurophysiological changes with age probed by inverse modeling of EEG spectra

S.J. van Albada [a,b,c,*], C.C. Kerr [a,b], A.K.I. Chiang [a,b], C.J. Rennie [a,b], P.A. Robinson [a,b,d]

[a] School of Physics, The University of Sydney, NSW 2006, Australia
[b] The Brain Dynamics Centre, Westmead Millennium Institute, Westmead Hospital and Western Clinical School of the University of Sydney, Westmead, NSW 2145, Australia
[c] Institute of Neuroscience and Medicine – Neuromodulation INM-7, Research Center Jülich, Leo-Brandt-Street, 52425 Jülich, Germany
[d] Faculty of Medicine, The University of Sydney, NSW 2006, Australia

ARTICLE INFO

Article history:
Accepted 22 September 2009
Available online 23 October 2009

Keywords:
Aging
EEG
Spectra
Mean-field model
Thalamus
Cortex

ABSTRACT

Objective: To investigate age-associated changes in physiologically-based EEG spectral parameters in the healthy population.
Methods: Eyes-closed EEG spectra of 1498 healthy subjects aged 6–86 years were fitted to a mean-field model of thalamocortical dynamics in a cross-sectional study. Parameters were synaptodendritic rates, cortical wave decay rates, connection strengths (gains), axonal delays for thalamocortical loops, and power normalizations. Age trends were approximated using smooth asymptotically linear functions with a single turning point. We also considered sex differences and relationships between model parameters and traditional quantitative EEG measures.
Results: The cross-sectional data suggest that changes tend to be most rapid in childhood, generally leveling off at age 15–20 years. Most gains decrease in magnitude with age, as does power normalization. Axonal and dendritic delays decrease in childhood and then increase. Axonal delays and gains show small but significant sex differences.
Conclusions: Mean-field brain modeling allows interpretation of age-associated EEG trends in terms of physiological processes, including the growth and regression of white matter, influencing axonal delays, and the establishment and pruning of synaptic connections, influencing gains.
Significance: This study demonstrates the feasibility of inverse modeling of EEG spectra as a noninvasive method for investigating large-scale corticothalamic dynamics, and provides a basis for future comparisons.

1. Introduction

Understanding the structural, chemical, and functional changes that accompany brain aging is one of the major goals of research in neuroscience. Structural changes are particularly rapid during childhood, slow down after adolescence, and appear to accelerate again in late adulthood. Although the morphological, chemical, and functional development of the human brain, as well as changes in the electroencephalogram (EEG), have been tracked extensively (Duffy et al., 1993; Gasser et al., 1988; Hartikainen et al., 1992; Kemper, 1994; Polich, 1997; Rossini et al., 2007; Thompson et al., 2000), knowledge of the specific processes underlying changes in the EEG across age is limited.

Growth and pruning processes affect the volumes of the cortical and subcortical gray matter, cerebral white matter, and the corpus callosum. Cranial size increases up to age ~20, with growth continuing a few years longer in males than in females (Dekaban, 1977; Eichorn and Bayley, 1962). Cortical gray matter volume increases up to adolescence (Giedd et al., 1999), although localized pruning already occurs during childhood (Caviness et al., 1996). The corpus callosum grows considerably between the ages of 3 and 11 years and more slowly up to 15 years (Thompson et al., 2000). Ongoing myelination increases the white matter content of various cortical and other brain areas throughout childhood (Barnea-Goraly et al., 2005; Perrin et al., 2008; Sowell et al., 2004).

After adolescence, a steady decrease in brain volume occurs, which appears to become more severe after about 60–70 years (Haug, 1987; Scahill et al., 2003). This is accompanied by an increase in absolute and relative cerebrospinal fluid volume that commences already in childhood (Gur et al., 1991; Sowell et al., 2002). Although reductions in brain volume were traditionally attributed to neuronal loss, later studies with improved methodology have largely failed to reveal loss of hippocampal or neocortical neurons with age, and have instead attributed decreased brain volume to shrinkage of neurons (Peters, 2002a; Rapp and Gallagher,

* Corresponding author. Address: Institute of Neuroscience and Medicine – Neuromodulation INM-7, Research Center Jülich, Leo-Brandt-Street, 52425 Jülich, Germany. Tel.: +49 2461 615366; fax: +49 2461 611880.
E-mail address: s.van.albada@fz-juelich.de (S.J. van Albada).

1388-2457/$36.00
doi:10.1016/j.clinph.2009.09.021

1996; Rasmussen et al., 1996). An exception is Pakkenberg and Gundersen (1997), who reported a loss of about 10% of neurons in the neocortex of both males and females between age 20 and 90. Thalamic volume also decreases with age, whether due to loss or shrinkage of neurons (Sullivan et al., 2004; van der Werf et al., 2001). Although some authors have reported white matter volume to be relatively stable compared to gray matter volume (Passe et al., 1997; Sullivan et al., 2004), others have found white matter volume reductions from about age 50 (Ge et al., 2002; Miller et al., 1980). According to a recent study, white matter shows much greater reductions than gray matter between the ages of 46 and 92 (Piguet et al., 2009).

Small numbers of neuritic plaques and neurofibrillary tangles, characteristic of Alzheimer's disease, accumulate even in normal aging (Morrison and Hof, 1997; Tomlinson et al., 1968). Often, advancing age is further accompanied by reductions in cerebral perfusion, oxygen consumption, and glucose utilization (Kuhl et al., 1982; Pantano et al., 1984; Zemcov et al., 1984). There are also age-related changes in chemical signaling (Gallagher and Colombo, 1995; McEntee and Crook, 1991; Suhara et al., 1991; Volkow et al., 2000).

There are sex differences in brain anatomy and chemistry, and in certain aspects of brain development (Coffey et al., 1998; Cosgrove et al., 2007; De Bellis et al., 2001). Female brains have smaller volumes and approximately 16% fewer neocortical neurons at any age than male brains (Caviness et al., 1996; Dekaban and Sadowsky, 1978; Haug, 1987; Pakkenberg and Gundersen, 1997). However, many studies have reported more substantial age-related atrophy or reductions in brain volume in men than in women (Coffey et al., 1998; Cowell et al., 1994; Gur et al., 1991; Tomlinson et al., 1968; Xu et al., 2000), although some have suggested earlier onset or more severe atrophy in women (Hatazawa et al., 1982; Hubbard and Anderson, 1983). It is generally found that a larger percentage of the total volume is occupied by gray matter in women than in men (Cosgrove et al., 2007).

This study aims to provide a new window on brain aging using a model of neuronal activity that incorporates the main structures and connections contributing to the EEG. This approach is based on a mean-field model of corticothalamic dynamics developed over a number of years, primarily by Robinson et al. (1997, 1998, 2001a, 2003), and Rennie et al. (1999, 2000, 2002). This model was partly based in turn on work by Nunez (1974, 1995), Wilson and Cowan (1972, 1973), Wright and Liley (1995), and others. Comparisons of model predictions with data have revealed good agreement with a range of features of EEGs, including evoked potentials (EPs) (Kerr et al., 2008), seizure dynamics (Breakspear et al., 2006; Roberts and Robinson, 2008), spectra (Robinson et al., 2001a; Rowe et al., 2004), coherence and correlations (Robinson, 2003), and changes with arousal (Robinson et al., 2002). Inverse modeling by fitting to spectra yields parameters including corticothalamic axonal delays, synaptodendritic rates, a damping rate for signals in the cortex, a scaling parameter for spectral power, and connection strengths of the cortex, thalamic relay nuclei, and thalamic reticular nucleus. An advantage of our model is that it provides information on structures as deep as the thalamus without the need for invasive measurements. Moreover, this information is of a different type than would be obtained by most invasive techniques, yielding average properties of large neuronal assemblies and their interconnections, rather than properties of small numbers of individual neurons.

Determining model parameters across age for healthy individuals is useful not only because it demonstrates the feasibility of extracting physiological information from the EEG, but also because it establishes a standard against which to compare clinical groups. Moreover, comparisons with known physiological changes provide a test of the model that can stimulate its further development.

In Section 2 we describe the subjects and data acquisition, the model, and the methods used for fitting and statistical analysis. Section 3 gives parameter values and age trends, and also addresses sex differences. Section 4 provides a summary and relates our results to the existing literature.

2. Methods

This section outlines the model and methods used in our analysis. Section 2.1 details the composition of the data set and criteria for inclusion. Section 2.2 provides an overview of the theoretical model of EEG generation. Section 2.3 summarizes the procedures for fitting model predictions to empirical spectra. Section 2.4 describes the statistical techniques used in the analysis of model parameters.

2.1. Subjects and EEG recording

The cross-sectional data set was composed of 763 males and 735 females, selected to have EEG and EP data across a range of electrodes, allowing future comparison with model fits to EPs (Kerr et al., in preparation), parameters obtained from deconvolution of EPs (Kerr et al., 2009), and detailed fits to alpha peaks (Chiang et al., in preparation). The 1498 subjects overlap with the 1008 previously studied by Williams et al. (2008). Subjects' ages were 6.4–86.6 years for males, and 6.1–82.6 years for females, with age distributions as shown in Fig. 1. The large number of young subjects allows reliable estimation of age trends over a period of relatively rapid change. Furthermore, the study also included 126 subjects aged 60 years or more, a larger number than considered in most studies of the EEG in aged individuals. All subjects were healthy, without any known history of brain injury; mental illness; substance abuse; psychological, psychiatric, neurological,

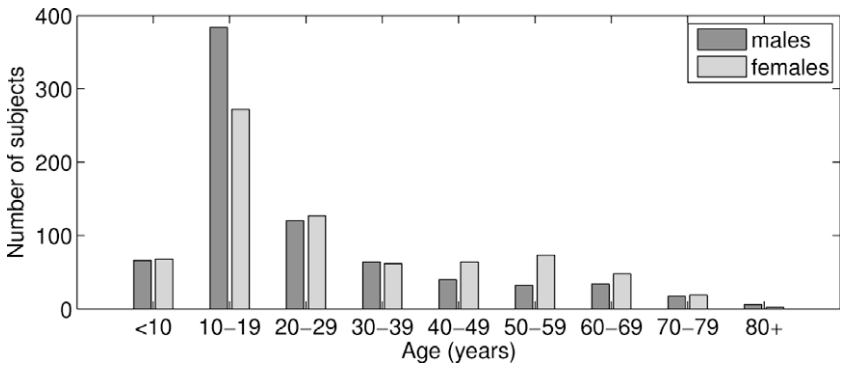

Fig. 1. Numbers of males and females in each age bin.

or genetic disorders; or other medical conditions that could influence the normality of the EEG. More detailed criteria were as in van Albada et al. (2007).

Eyes-closed resting EEGs were recorded by Brain Resource Ltd. (www.brainresource.com) and made available through the Brain Resource International Database (BRID) (Gordon et al., 2005). Recordings were obtained with a NuAmps amplifier (Neuroscan) at 26 electrode sites according to an extended International 10–20 system. The sampling rate was 500 Hz and average of mastoids was used as a reference. To keep the scope of the study manageable, a single electrode was selected for further analysis. The Cz electrode was chosen, as this electrode is relatively unaffected by muscle artifact (Saunders, 1979). Data were corrected offline for eye movements using a method based on that of Gratton et al. (1983). A 100 Hz low-pass filter was applied to two minutes of relatively artifact-free EEG. The spectrum was calculated at intervals of 0.25 Hz by averaging the spectra of successive 4 s epochs multiplied by a Welch window. Two minutes of EEG were considered sufficient for two reasons. First, the large number of subjects allows reliable estimation of average age trends even with relatively short recordings. Second, the reproducibility of spectral parameters is not greatly improved by using longer recordings (Gasser et al., 1985; Salinsky et al., 1991; van Albada et al., 2007).

2.2. Theoretical model

A schematic diagram of the neuronal populations included in the model, and their interconnections, is given in Fig. 2. Within the cortex, the model includes excitatory pyramidal cells, which project both intracortically and to the thalamus, and short-range inhibitory interneurons. The subscripts e and i are used to represent the excitatory and inhibitory cortical populations. The thalamic relay and reticular nuclei are respectively denoted by the subscripts s and r. Input from the brainstem to the thalamus is indicated by the subscript n. With each connection is associated a gain G_{ab} quantifying the number of additional pulses out per additional pulse in with respect to the steady state, where b is the sending and a is the receiving population. Loop gains are combined into the products $G_{srs} = G_{sr}G_{rs}$ for the loop between thalamic reticular and relay nuclei; $G_{ese} = G_{es}G_{se}$ for the corticothalamic loop passing only through the relay nuclei; and $G_{esre} = G_{es}G_{sr}G_{re}$ for the corticothalamic loop also passing through the reticular nucleus. These gains and the corresponding loops are illustrated in Fig. 2.

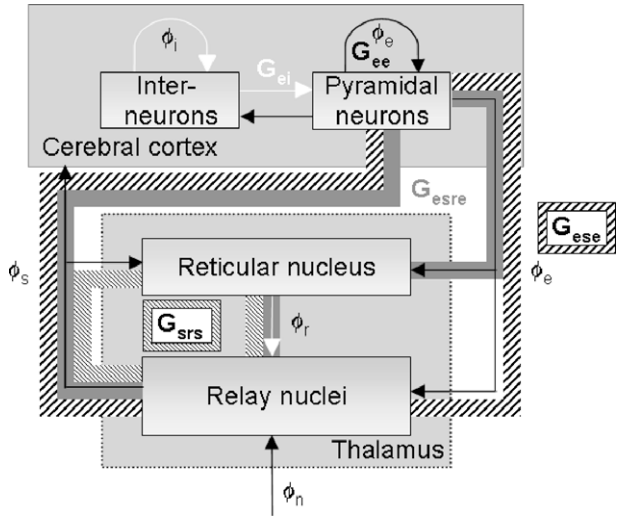

Fig. 2. Schematic representation of the model components and their interconnections: e = cortical excitatory (pyramidal) neurons, i = cortical inhibitory neurons, s = thalamic (specific and secondary) relay nuclei, r = thalamic reticular nucleus. External input to the thalamus is given by ϕ_n. The connections or loops associated with each gain are also indicated: intracortical excitatory and inhibitory connections (G_{ee} and G_{ei}), the direct and indirect corticothalamic loops (G_{ese} and G_{esre}), and the intrathalamic loop (G_{srs}). Black arrows indicate excitatory connections; white arrows inhibitory ones.

Full details of the model have been published elsewhere (Robinson et al., 1997, 1998, 2001a, 2002), but the equations are given in the Appendix for completeness. These enable frequency spectra to be computed from basic physiological quantities, of which we consider those that were allowed to vary when fitting the model to empirical EEG spectra. Besides the gains listed above, these quantities are: t_0, the axonal delay associated with the direct corticothalamic loop; α, a characteristic decay rate of the cell-body potential after synaptic input (an average or effective value across neural populations); γ, a damping rate associated with propagation of waves of activity along the cortex; and p_0, a normalization for the frequency spectrum. All parameters are listed in Table 1.

The parameters considered here differ from traditional qEEG measures in their direct connection with physiological quantities. As such, they can provide a useful complement to traditional qEEG, especially if physiological models of EEG generation are further developed. Apart from physiological interpretations, an advantage of the model parameters is that they capture spectral shape within frequency bands, which is not captured by band powers.

2.3. Model fitting

As described in Rowe et al. (2004) and van Albada et al. (2007), the natural logarithm of the dimensionless version of the spectral power (otherwise measured in μV^2/Hz) was fitted to the empirical log-transformed spectrum using the Levenberg–Marquardt method (Press et al., 1992), which minimizes the χ^2 error defined by

$$\chi^2 = \sum_{i=1}^{N} \frac{[\ln(P_{emp,i}) - \ln(P_{the,i})]^2}{\sigma_i^2}, \quad (1)$$

where $P_{emp,i}$ is the empirical spectrum, and σ_i is the standard deviation of $\ln P_{emp}$ for frequency index i. Frequencies up to 50 Hz were taken into account, but the power around 50 Hz was weighted with large σ to downplay the contribution of points contaminated by mains power. Fitting followed a Monte Carlo method in which the ten fitted parameters were repeatedly initialized randomly and the model fitted, until 30 convergent fits were obtained. The stopping criterion for the fitting routine was $\Delta\chi^2 < 10^{-5}$ for six successive iterations. Of 1661 subjects' spectra, 1568 were successfully fitted (94%). To obtain a single subject set for which model parameters, EPs (Kerr et al., in preparation), and alpha peak data across sites (Chiang et al., in preparation) could be investigated, we selected from the set of 1568 subjects the 1498 subjects with EP data for a large number of electrodes. All these subjects also had EEG spectral data across sites, from which alpha peak parameters could be extracted. Fig. 3 gives illustrative examples of fits with different values of χ^2. The values of χ^2 were larger than those reported in Rowe et al. (2004) due to a different normalization of weights, but this did not substantially affect the fits obtained.

2.4. Statistical analysis

The statistical analysis was carried out using R Version 2.7.0 (R Development Core Team, 2005). Visual inspection of histograms and a Shapiro–Wilk test for normality (Shapiro and Wilk, 1965) revealed that none of the parameters were normally distributed ($p < 1.0e-7$). Furthermore, the residuals of parametric linear regression of model parameters versus age were non-normal ($p < 1.0e-14$). Therefore, nonparametric methods were used except where indicated otherwise.

Table 1
Parameters of the corticothalamic model used to fit theoretical predictions to empirical EEG spectra. Parameters considered in this study are marked by an asterisk. The minimum and maximum values are soft boundaries created by imposing a smoothly increasing penalty for smaller or larger values.

Parameter	Unit	Description	Value	Min.	Max.
$*\alpha$	s^{-1}	Decay rate of cell-body potential		10	200
β	s^{-1}	Rise rate of cell-body potential	4α		
r_e	mm	Range of pyramidal axons	80		
v_e	ms^{-1}	Propagation speed along pyramidal axons	γr_e		
$*\gamma$	s^{-1}	Cortical damping rate		40	280
$*t_0$	ms	Corticothalamic axonal latency		60	130
$*G_{ee} = G_{ie}$	–	Excitatory cortical gain		0	20
$*G_{ei} = G_{ii}$	–	Inhibitory cortical gain		−35	1
$*G_{ese}$	–	Gain for direct corticothalamic loop		0	20
$*G_{esre}$	–	Gain for indirect corticothalamic loop passing through the thalamic reticular nucleus		−30	2
$*G_{srs}$	–	Gain for intrathalamic loop		−15	0.5
$*p_0$	–	Normalization for spectrum		No limits	
k_0	m^{-1}	Cut-off wavenumber for spatial filtering	37.5		
L_x, L_y	m	Linear dimensions of cortex	0.5		
A_{EMG}	$\mu V^2\,Hz^{-1}$	Amplitude of EMG component		0	10
ω_{EMG}	Hz	Peak frequency of EMG component	$2\pi \times 40$		

First, the robustness of fits was investigated by refitting empirical spectra with noise added. White Gaussian noise with standard deviation 0.2 was added to log-transformed spectra (using the dimensionless version of power in $\mu V^2\,Hz^{-1}$). This process was repeated to obtain spectra with ten different noise levels. Robustness analysis was restricted to the 1126 cases for which refitting was successful at all noise levels. The standard deviation of the first set of noisy spectra approximates the standard error of ln power of 2-minute spectra computed from 4-second segments (not shown), which corresponds to the method used here (cf. Section 2.1). Thus, the robustness of model parameters was assessed by calculating Spearman correlations between parameters for the original fits and those for the first set of noisy spectra. Spearman correlations for between-fit differences were also determined for each pair of parameters. This gave an indication of correlations induced by fitting (in the presence of uncertainty or noise) rather than physiology. To check for any consistent bias introduced by uncertainty or noise, parametric linear regression was performed of mean parameter values versus noise level.

For the original fits, sex differences in model parameters were assessed using the Mann–Whitney test for independent samples (Hollander and Wolfe, 1973). We compared means and distributions of model parameters with those obtained using a previous version of the fitting routine (Rowe et al., 2004), and those reported in a longitudinal study of healthy males in the age range 18–28 years (van Albada et al., 2007).

Age trends were approximated using a functional form that was chosen based on the following observations: (i) trends were often approximately linear in young and old age; (ii) there was substantial variation in the age ranges over which trends were nonlinear; (iii) the transition from "development" to "aging" occurs gradually, with intermediate slopes in early adulthood; and (iv) the median did not clearly show more than one turning point for any of the parameters. This motivated a fitting function that is smooth,

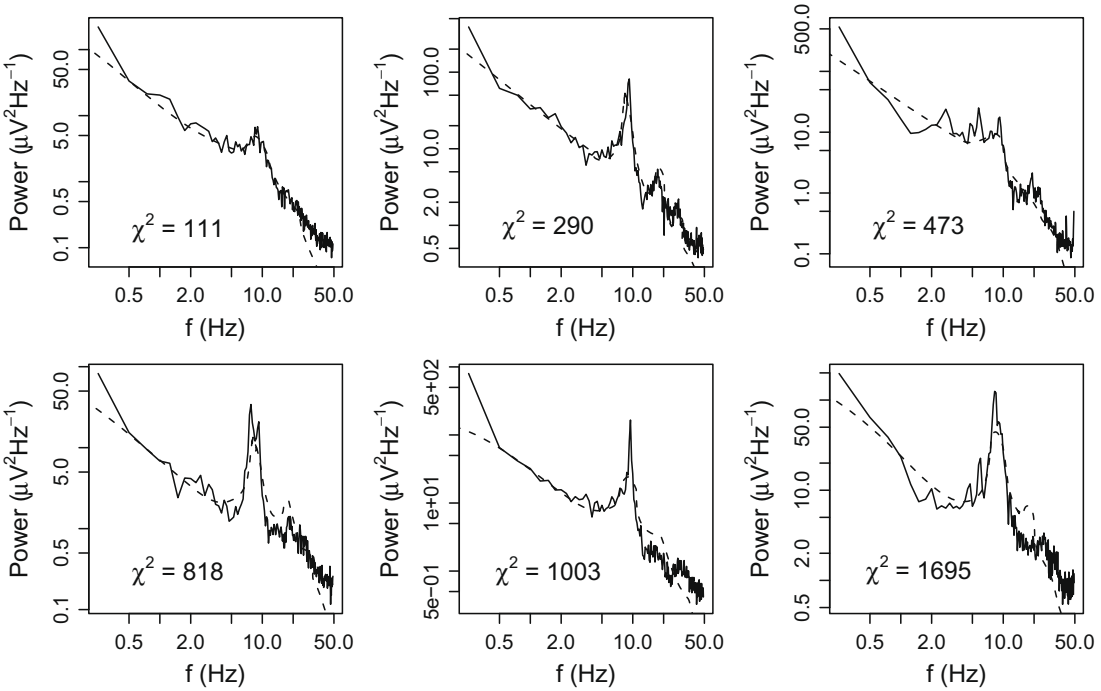

Fig. 3. Examples of experimental (solid) and corresponding model spectra (dashed) from single subjects with varying goodness of fit.

asymptotically linear, and has a second derivative of constant sign. A functional form that meets these criteria and has only a small number of parameters is given by

$$y = Cx + (C - A)\tau \ln\left(1 + \exp[-(x - I)/\tau]\right) + D, \quad (2)$$

$$I = \frac{B - D}{C - A}, \quad (3)$$

where x is the age, τ is a width parameter quantifying the age range over which the slope changes considerably, and A, B, C, and D are parameters representing asymptotic slopes and intercepts. Since fits were relatively insensitive to τ, this parameter was fixed at 3 years, which yielded good fits. Eq. (2) represents a smooth interpolation between two straight lines, $y = Ax + B$ for $x \to -\infty$ and $y = Cx + D$ for $x \to \infty$. These lines intersect at I, which is also the point of maximum rate of change in slope for the interpolated fit. The fits display a minimum or maximum at

$$x = I - \tau \ln\left(-\frac{C}{A}\right), \quad (4)$$

if A and C have opposite sign. More than one turning point is excluded, because the second derivative of (2) is always negative when $A > C$, strictly positive when $A < C$, and zero when $A = C$. The function (2) is illustrated in Fig. 4.

In order to track the median, fits were performed by minimizing the mean absolute difference between fitted and measured values. Optimization was achieved using a downhill simplex method (Nelder and Mead, 1965), with starting conditions fine-tuned to obtain close fits to moving medians computed for groups of 100 subjects with steps of 10 subjects. Confidence intervals for the parameters and fits were obtained by bootstrapping with 1000 resamplings.

For comparison with the literature, we also considered age trends of the form (2) in 'raw' empirical spectra. Band powers were determined in the ranges 0.5–4 Hz (delta), 4.25–8 Hz (theta), 8.25–12 Hz (alpha), 12.25–30 Hz (beta), and 30.25–49.5 Hz (gamma). Total power was the sum of these band powers, and relative powers were absolute power divided by total power. Dominant alpha frequencies were determined from spectra at a range of electrodes using the method of Chiang et al. (2008). We consider mainly the Cz electrode, for which 1212 subjects exhibited a clear peak, but we compare with other sites where relevant.

We also investigated the sensitivity of qEEG parameters to model parameters. Normally distributed values with mean zero and standard deviation 0.25 times the sample standard deviation were added to fitted model parameters, and spectra were recomputed. Differences between qEEG parameters for the original and modified spectra were computed, where 0.01 Hz resolution was used to determine alpha peak frequencies. We then calculated Spearman correlations between differences in model parameters and differences in qEEG parameters. The sensitivity of alpha peak frequencies was only investigated for the 1212 subjects whose empirical Cz spectra showed clear peaks. The use of fitted, rather than randomly chosen, parameters ensured that physiologically representative spectra were considered. Artificially varied spectra have the advantage over spectra taken directly from the sample under study that qEEG-model parameter correlations are not confounded by age trends and noise.

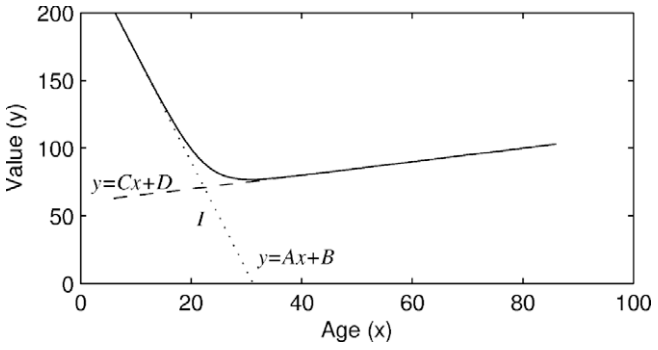

Fig. 4. Example of a function of the form (2) with negative A and positive C (solid line). The asymptotic linear trends $y = Ax + B$ (dotted) and $y = Cx + D$ (dashed) intersect at $x = I$.

3. Results

The robustness of fitted model parameters is discussed in Section 3.1. Parameter distributions are given in Section 3.2 and compared to previously published results. Age trends in fitted and model-free spectral parameters are presented in Section 3.3.

3.1. Robustness of fits

Fig. 5 shows the noise dependence of mean parameter values for the 1126 subjects whose spectra were successfully fitted at all noise levels. To a good approximation, all means depend linearly on the noise variance. The absolute values of all parameters except α tend to be overestimated in the presence of noise. However, the degree of overestimation is about two orders of magnitude smaller than the standard deviation of each parameter, so spectral uncertainty does not substantially bias fitted parameter values.

Table 2 shows the results of comparing original parameter values with those obtained after adding noise to empirical spectra. The last column of Table 2 lists correlations between parameter values for the original fits and those obtained from the first set of noisy spectra. These correlations indicate that, overall, parameters are robustly fitted. The most robust parameter is G_{srs} ($\rho = 0.96$), while G_{ei} is the least robust ($\rho = 0.79$). The corticothalamic loop delay t_0 shows the least interaction with other parameters.

It is seen from Table 2 that almost all parameter pairs show interactions due to noise. Consequently, age trends of physiological origin in some parameters may cause artificial age trends in other (especially less robust) parameters. Particularly strong correlations are found for between-fit differences in p_0 and G_{ei} ($\rho = -0.86$), G_{ese} and G_{esre} ($\rho = -0.74$), and G_{ee} and G_{ei} ($\rho = -0.62$). This should be kept in mind when interpreting the results in the following sections.

3.2. Parameter values

Parameter distributions are shown in Fig. 6. Table 3 lists parameter means and standard deviations, and χ^2-values The corticothalamic loop gains G_{ese} and G_{esre} were both stronger (i.e., larger in magnitude) in males. The intrathalamic loop, represented by the gain G_{srs}, was stronger in females. The corticothalamic loop delay t_0 was on average slightly longer in females. No significant differences were found in the intracortical gains G_{ee} and G_{ei}, or in the parameters α, γ, and p_0. Fits were on average slightly better for females than for males, as indicated by lower values of χ^2.

Dominant alpha frequencies are expected to be approximately inversely proportional to t_0 (Robinson et al., 2002). However, the sex difference in t_0 did not translate into a significant sex difference in alpha peak frequencies averaged across age (males, 9.5 Hz; females, 9.4 Hz; $p = 0.30$). Boys up to age 16 did show significantly higher peak frequencies than girls in this age range (boys, 9.6 Hz; girls, 9.3 Hz; $p = 0.0045$), and had significantly lower values of t_0 (boys, 77 ms; girls, 81 ms; $p = 1.0e-5$). In contrast, females aged 16–24 years had higher peak frequencies (females,

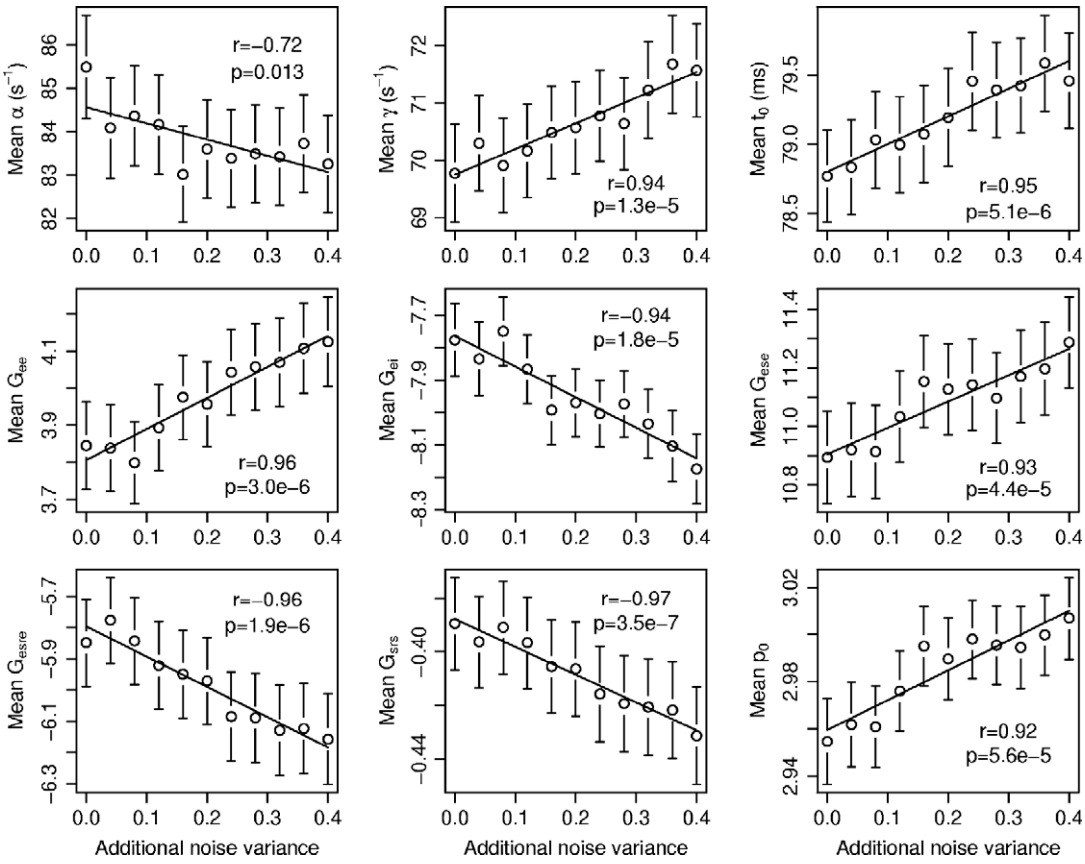

Fig. 5. Dependence of mean parameter values on noise in spectra. Data for the original fits are plotted at zero noise variance. Error bars indicate SEMs. Linear regression fits and Pearson correlation coefficients are shown, with corresponding significance values.

9.7 Hz; males, 9.4 Hz; $p = 0.0028$), despite a lack of difference in t_0 (females, 78 ms; males, 77 ms; $p = 0.76$). The same pattern of sex differences in alpha peak frequencies was found at occipital sites. We did not find significant sex differences in t_0 or Cz alpha peak frequencies in aged individuals, but frontal rhythms occurred at significantly lower frequencies in women than in men above about age 70. These issues are explored further by Chiang et al. (in preparation).

Rowe et al. (2004) reported distributions of model parameters for eyes-open and eyes-closed spectra of 100 healthy subjects (49 females, mean age 44 years, SD 15 years; and 51 males, mean age 45 years, SD 16 years) using an earlier version of the fitting routine. Compared to the eyes-closed distributions in that paper, our sample yielded larger standard deviations for all parameters except t_0 and γ. The mean values of γ, t_0, G_{ee}, and $|G_{srs}|$ were smaller than those in Rowe et al. (2004), whereas α, $|G_{ei}|$, G_{ese}, $|G_{esre}|$, and p_0 were found to be larger on average. We attribute this to the different fitting algorithms used, since the new algorithm runs through a range of initial values, whereas the version used by Rowe et al. (2004) initialized parameters at a single set of values. The new fitting algorithm is an improvement over the old one because it reduces bias introduced by the choice of initialization.

We previously reported classic and model-based spectral parameters for 32 healthy males aged 18–28, whose eyes-closed

Table 2
Robustness of model parameters, assessed by adding noise to empirical spectra and refitting. The second through tenth columns contain rank correlations for differences in parameters between the original fits and those obtained from spectra with added Gaussian noise with standard deviation 0.2 on a log scale (in upper triangular form). Corresponding significance values are listed below the diagonal. These correlations obey $\rho(x_1 - x_2, y_1 - y_2) = \rho(y_1 - y_2, x_1 - x_2)$ for parameters x and y, and fits 1 and 2. The last column indicates rank correlations between fits before and after adding noise.

Parameter	α	γ	t_0	G_{ee}	G_{ei}	G_{ese}	G_{esre}	G_{srs}	p_0	ρ
α	1	−0.40	0.059	−0.23	0.22	0.011	−0.19	0.59	−0.41	0.91
γ	***	1	−0.078	0.22	−0.14	−0.29	0.36	−0.29	0.010	0.85
t_0	*	**	1	−0.015	0.020	−0.00087	−0.017	0.038	−0.0037	0.92
G_{ee}	***	***	n.s.	1	−0.62	0.29	−0.37	−0.34	0.49	0.90
G_{ei}	***	***	n.s.	***	1	−0.59	0.33	0.076	−0.86	0.79
G_{ese}	n.s.	***	n.s.	***	***	1	−0.74	0.082	0.60	0.82
G_{esre}	***	***	n.s.	***	***	***	1	−0.13	−0.27	0.87
G_{srs}	***	***	n.s.	***	*	**	***	1	−0.20	0.96
p_0	***	n.s.	n.s.	***	***	***	***	***	1	0.88

Significance levels: n.s., not significant.
* 0.05.
** 0.01.
*** 0.001.

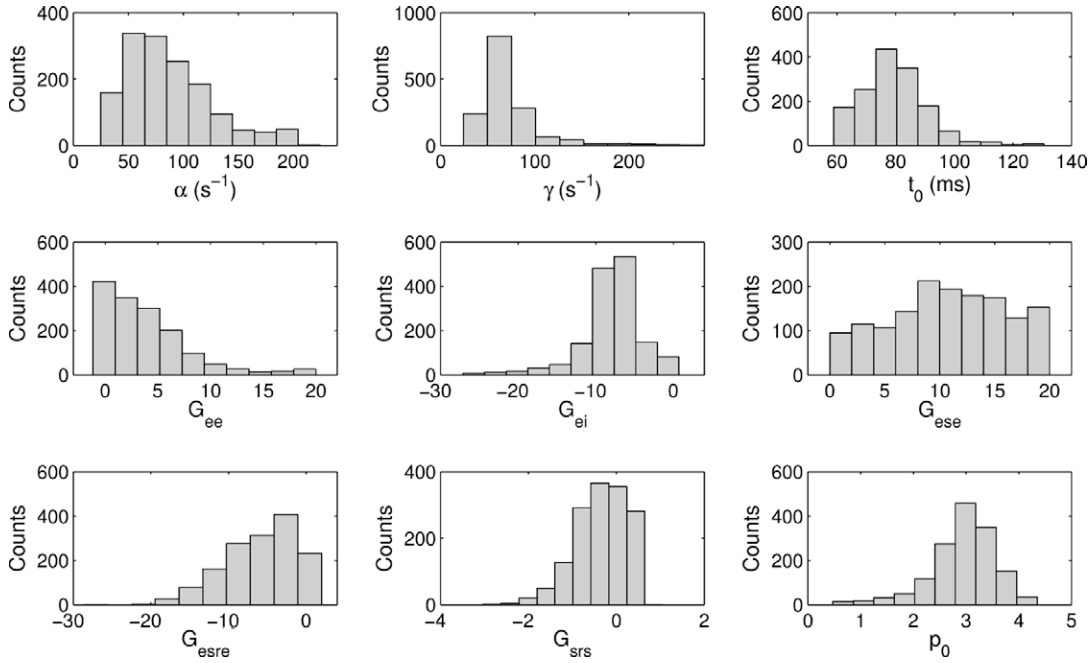

Fig. 6. Histograms of model parameters.

EEGs were obtained in six consecutive weeks, followed for some subjects by intervals of several months (van Albada et al., 2007). Mean values for males in the range 18–28 years from the present study are compared with those from van Albada et al. (2007) in Table 3. Overall, differences between the two studies are small, and only G_{ee} and p_0 differ substantially.

3.3. Age trends

Section 3.3.1 considers changes in model parameters across age. For comparison, trends in qEEG parameters are described in Section 3.3.2.

3.3.1. Model parameters

Fig. 7 shows scatter plots and fitted nonlinear age trends of the form (2) for model parameters. The fits closely follow moving medians. Age trends for males and females are compared in Fig. 8. The parameters for each of these fits are listed along with their standard errors in Table 4. The parameter I is also indicated, corresponding to the age of the bend in the regression. Note that the slopes listed are asymptotic values, and differ somewhat from slopes during development and aging.

Trends in α and t_0 are characterized by steep decreases followed by more gradual increases after age ~15 years. The cortical wave decay rate γ increases up to about age 20 years, after which the trend levels off. All gains except G_{srs} decrease in absolute value with age, changes occurring most rapidly during childhood. The power normalization parameter p_0 shows a rapid decline up to age ~20 years, with much slower reductions thereafter.

These trends are similar for males and females, although there are some differences (cf. Fig. 8). Girls have slightly larger values of t_0 than boys, but the values reconverge after adolescence. Females show an increase in G_{ese} at least up to age 20, whereas males show a decrease in this parameter over the same age range. Almost the reverse is true for G_{esre}, which becomes weaker in boys but remains approximately constant in girls. Recalling that spectral

Table 3
Means and SEMs for model parameters and χ^2. Units are as in Table 1. Standard deviations are about 39 times as large as the standard errors listed. Mean$_R$ denotes means for the eyes-closed state from Rowe et al. (2004). The column labeled 'p-value' lists results of the Mann–Whitney test comparing males and females. Values for males in the range 18–28 years are compared between the present study and van Albada et al. (2007) (Mean$_A$) in the last two columns, and the Mann–Whitney test was used to check for significant differences.

Parameter	All subjects		Males	Females	p-value	Mean 18–28	Mean$_A$
	Mean	Mean$_R$	Mean	Mean			
α	88 ± 1	75	88 ± 1	87.3 ± 1.0	0.98	84	75
γ	71.8 ± 0.8	140	71.6 ± 0.8	72.1 ± 0.8	0.22	81	77
t_0	79.2 ± 0.3	84	78.1 ± 0.3	80.3 ± 0.3	1.2e − 5***	77	79
G_{ee}	3.8 ± 0.1	5.8	3.9 ± 0.1	3.8 ± 0.1	0.67	3.2	4.1*
G_{ei}	−8.0 ± 0.1	−7.5	−8.04 ± 0.10	−7.9 ± 0.1	0.14	−7.7	−8.4
G_{ese}	10.8 ± 0.1	5.4	11.2 ± 0.1	10.3 ± 0.1	2.5e − 4***	11.3	11.7
G_{esre}	−5.7 ± 0.1	−3.3	−6.3 ± 0.1	−5.2 ± 0.1	3.0e − 6***	−5.7	−6.2
G_{srs}	−0.34 ± 0.02	−0.50	−0.29 ± 0.01	−0.40 ± 0.02	1.5e − 4***	−0.32	−0.39
p_0	2.94 ± 0.02	2.49	2.92 ± 0.02	2.96 ± 0.02	0.079	2.80	2.98**
χ^2	360 ± 10		370 ± 10	340 ± 10	1.7e − 4***		

Significance levels:
* 0.05.
** 0.01.
*** 0.001.

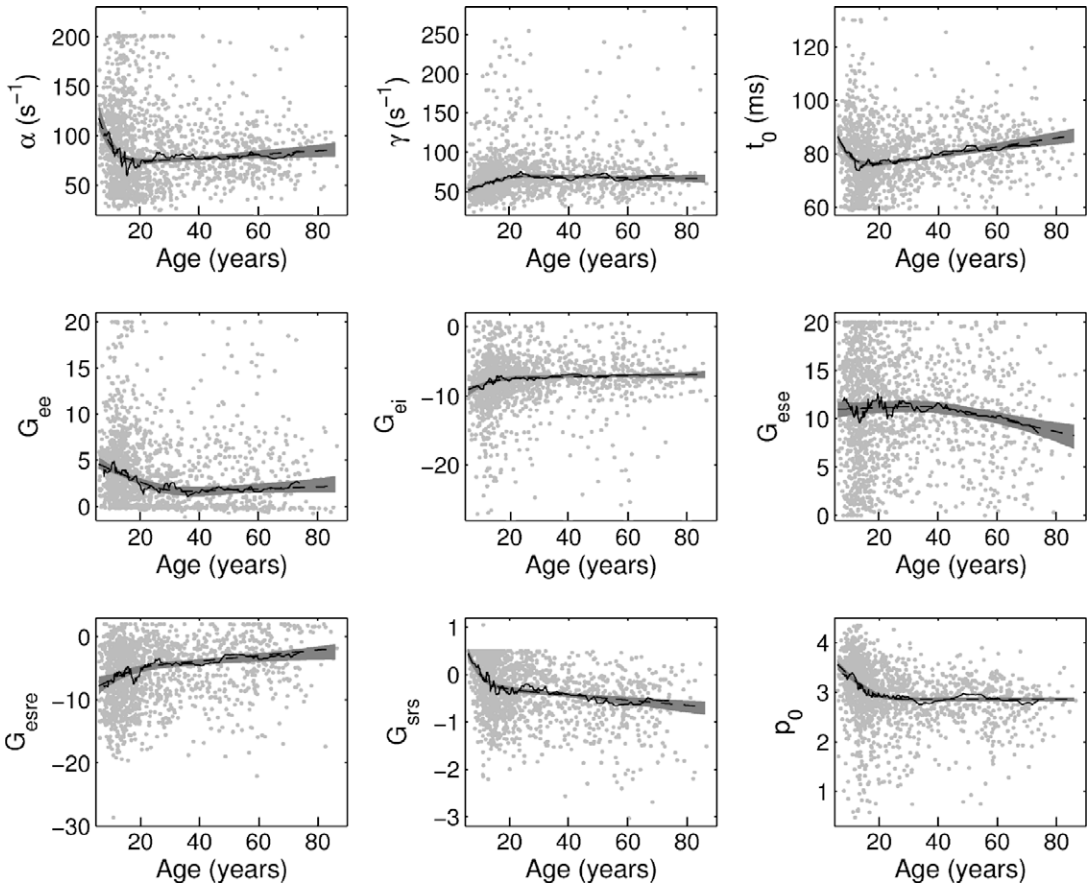

Fig. 7. Scatter plots and age trends of model parameters. Solid lines indicate moving medians, while dashed lines indicate fits of the form (2). The gray patches represent 95% confidence intervals for the fits, obtained by bootstrapping.

uncertainty links changes in G_{ese} to opposite changes in G_{esre} (cf. Table 2), some of these differences may not properly reflect the underlying physiology. Similarly, G_{srs} declines more with age in females than in males, while p_0 shows a greater decline in males, although the sex difference in correlation coefficients after age 20 was not found to be statistically significant [z-test (Olkin and Finn, 1995); $p = 0.32$]. Spectral uncertainty also induces a negative correlation between these quantities, albeit to a lesser extent than between G_{ese} and G_{esre} (cf. Table 2). Fig. 8 shows that p_0 levels off to higher values in females than in males, and average values of this parameter in subjects > 18 years differ significantly across sex (males, 2.7; females, 2.9; $p = 4.3\text{e}-5$).

3.3.2. Comparison with model-free spectral measures

Empirical and fitted model spectra across age are shown in Fig. 9. For the contour plots in Fig. 9a and c one-year intervals were used between ages 6 and 20, five-year intervals from 20 to 80, and a single band for age $\geqslant 80$. Fig. 9b and d show empirical and fitted model spectra for a coarser set of age bands. Fig. 10 contains age trends of the form (2) in empirical qEEG parameters.

Total power, and especially that at low frequencies, decreases with age at a gradually diminishing rate. Thus, relative low-frequency power is reduced, and relative high-frequency power is enhanced. Relative alpha power increases approximately until age 30 and then decreases. The frequency of the alpha peak rises until adolescence and then decreases into old age. Since some alpha peaks, particularly in children and the elderly, appear in what has been defined here to be the theta range (i.e., corresponding to adult theta frequencies), this will contribute to the observed trends in relative theta and alpha power. Fig. 9 shows that a small beta peak develops from about age 40, when alpha peaks are sharper than in early life. The parallel development of beta peaks and sharper alpha peaks supports the hypothesis, implied by our model, that beta is an approximate harmonic of alpha (Robinson et al., 2001a). Note from Fig. 9b that there is even a hint of a third harmonic between 20 and 30 Hz in older subjects.

Table 5 illustrates the sensitivity of model spectra to model parameters, based on variations around fitted values. Higher synaptodendritic and cortical decay rates α and γ are associated with more power in the alpha through gamma bands. Thus, larger α and γ increase relative high-frequency power and reduce relative low-frequency power. Greater intracortical excitation, quantified by G_{ee}, has the opposite effect. As expected, p_0 does not affect any of the relative band powers, but is positively correlated with absolute power in all bands. The correlations are not perfect because all parameters were varied simultaneously. Of model parameters besides p_0, G_{ei} is most strongly correlated with absolute power in the delta through beta bands. Stronger intracortical inhibition is associated with less power in all bands. Stronger G_{ese} enhances relative alpha power, since the model describes alpha resonances that arise in corticothalamic loops. Relative delta power depends most consistently on the intrathalamic gain G_{srs}: less negative G_{srs} is associated with more relative delta power. Higher rates α and γ, and shorter corticothalamic axonal loop delays t_0, are predictive of higher alpha peak frequencies (cf. Section 2.2). The gains G_{ee}, G_{esre}, and G_{srs} have a significant negative correlation with alpha peak frequency. Thus, stronger intrathalamic interactions and weaker intracortical excitation are associated with higher peak frequencies. Relative theta power has a significant positive correlation with t_0, since sufficiently large t_0 can move alpha peaks to the theta range.

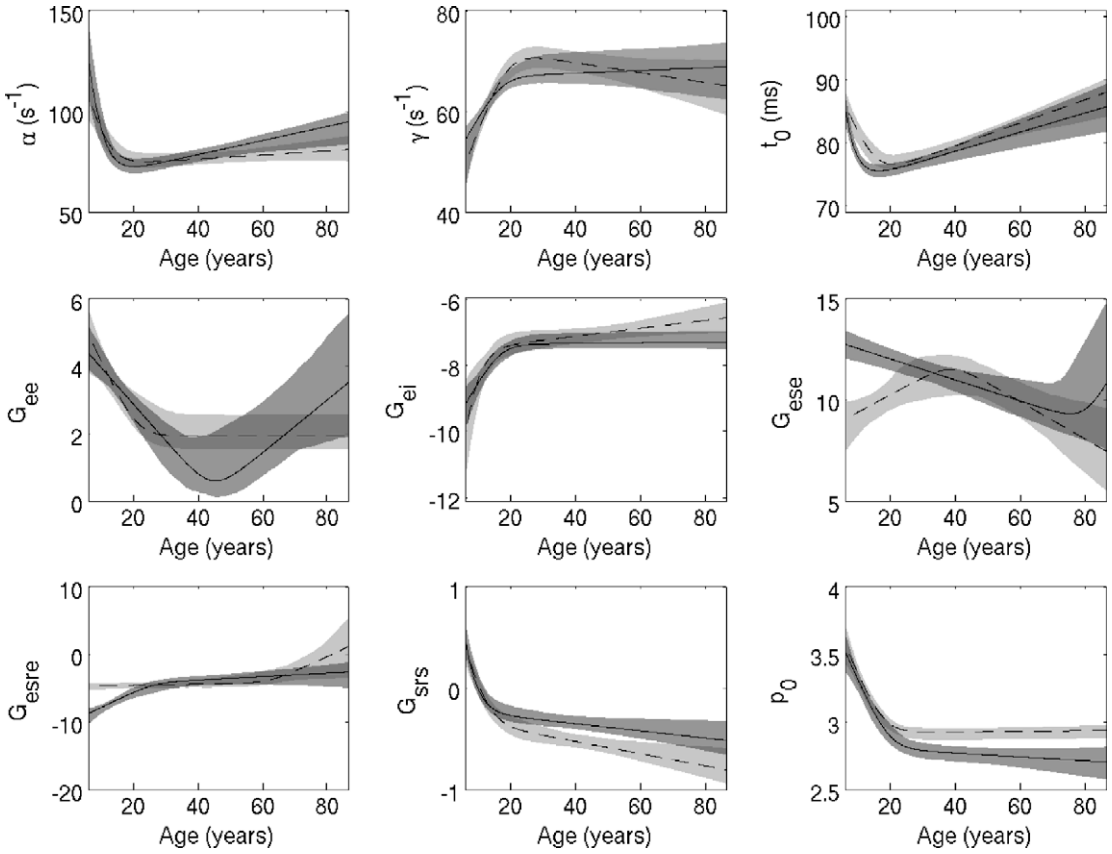

Fig. 8. Age trends in model parameters for males (solid lines) and females (dashed lines), with corresponding 95% confidence intervals.

Table 4
Parameters (A–D) and their standard errors for age trends of the form (2). The parameter $I = (B - D)/(C - A)$, representing the age (in years) of the turning point in each age trend, is also given along with its standard error. The numbers of figures reported are adapted to the corresponding standard errors. Slopes that differ significantly from zero based on 95% bootstrapping intervals are indicated in bold.

Parameter	A	B	C	D	I
All subjects					
α	**−12 ± 4**	180 ± 20	**0.18 ± 0.06**	71 ± 3	9 ± 3
γ	**1.4 ± 0.4**	43 ± 4	−0.06 ± 0.05	71 ± 2	19 ± 5
t_0	**−4 ± 1**	104 ± 4	**0.16 ± 0.02**	72.8 ± 0.8	8 ± 2
G_{ee}	**−0.14 ± 0.03**	5.4 ± 0.5	0.01 ± 0.01	1.3 ± 0.7	28 ± 9
G_{ei}	**0.17 ± 0.07**	−10.1 ± 0.7	0.008 ± 0.005	−7.6 ± 0.2	15 ± 8
G_{ese}	0.01 ± 0.02	10.9 ± 0.6	**−0.07 ± 0.02**	14 ± 2	40 ± 30
G_{esre}	**0.2 ± 0.1**	−9 ± 2	**0.04 ± 0.01**	−5.6 ± 0.5	20 ± 20
G_{srs}	**−0.22 ± 0.06**	1.5 ± 0.2	**−0.005 ± 0.001**	−0.21 ± 0.05	8 ± 2
p_0	**−0.059 ± 0.009**	3.91 ± 0.09	5e − 5 ± 3e − 5	2.85 ± 0.02	18 ± 3
Males					
α	**−16 ± 5**	210 ± 20	**0.35 ± 0.08**	65 ± 3	9 ± 3
γ	**1.2 ± 0.8**	48 ± 7	0.03 ± 0.04	67 ± 2	20 ± 10
t_0	**−13** ± 3	111 ± 8	**0.15 ± 0.03**	72.7 ± 0.9	3.0 ± 1.0
G_{ee}	**−0.11 ± 0.03**	5.1 ± 0.5	**0.08 ± 0.03**	−3 ± 2	40 ± 10
G_{ei}	**0.17 ± 0.06**	−10.2 ± 0.6	0.001 ± 0.001	−7.4 ± 0.1	16 ± 7
G_{ese}	**−0.05 ± 0.01**	13.1 ± 0.5	**0.31 ± 0.07**	−16 ± 4	80 ± 20
G_{esre}	**0.23 ± 0.09**	−10 ± 1	0.03 ± 0.02	−4.7 ± 0.9	30 ± 10
G_{srs}	**−0.3 ± 0.1**	1.8 ± 0.3	**−0.004 ± 0.002**	−0.20 ± 0.06	6 ± 2
p_0	**−0.05 ± 0.01**	3.9 ± 0.1	−0.001 ± 0.001	2.83 ± 0.05	19 ± 5
Females					
α	**−5 ± 3**	140 ± 20	0.10 ± 0.07	73 ± 3	12 ± 7
γ	**1.7 ± 0.4**	39 ± 4	**−0.10 ± 0.05**	74 ± 2	19 ± 5
t_0	**−1.2 ± 0.5**	93 ± 3	**0.18 ± 0.03**	72 ± 1	15 ± 6
G_{ee}	**−0.20 ± 0.06**	6.2 ± 0.8	0.0005 ± 0.0007	1.9 ± 0.3	21 ± 8
G_{ei}	**0.9 ± 0.4**	−14 ± 2	**0.012 ± 0.005**	−7.6 ± 0.3	7 ± 4
G_{ese}	**0.09 ± 0.06**	8.6 ± 0.9	**−0.09 ± 0.03**	15 ± 2	40 ± 20
G_{esre}	0.008 ± 0.010	−4.6 ± 0.3	**0.2 ± 0.1**	−20 ± 10	60 ± 60
G_{srs}	**−0.10 ± 0.03**	1.0 ± 0.2	**−0.006 ± 0.002**	−0.28 ± 0.09	13 ± 5
p_0	**−0.06 ± 0.01**	3.9 ± 0.1	0.0003 ± 0.0002	2.92 ± 0.02	17 ± 5

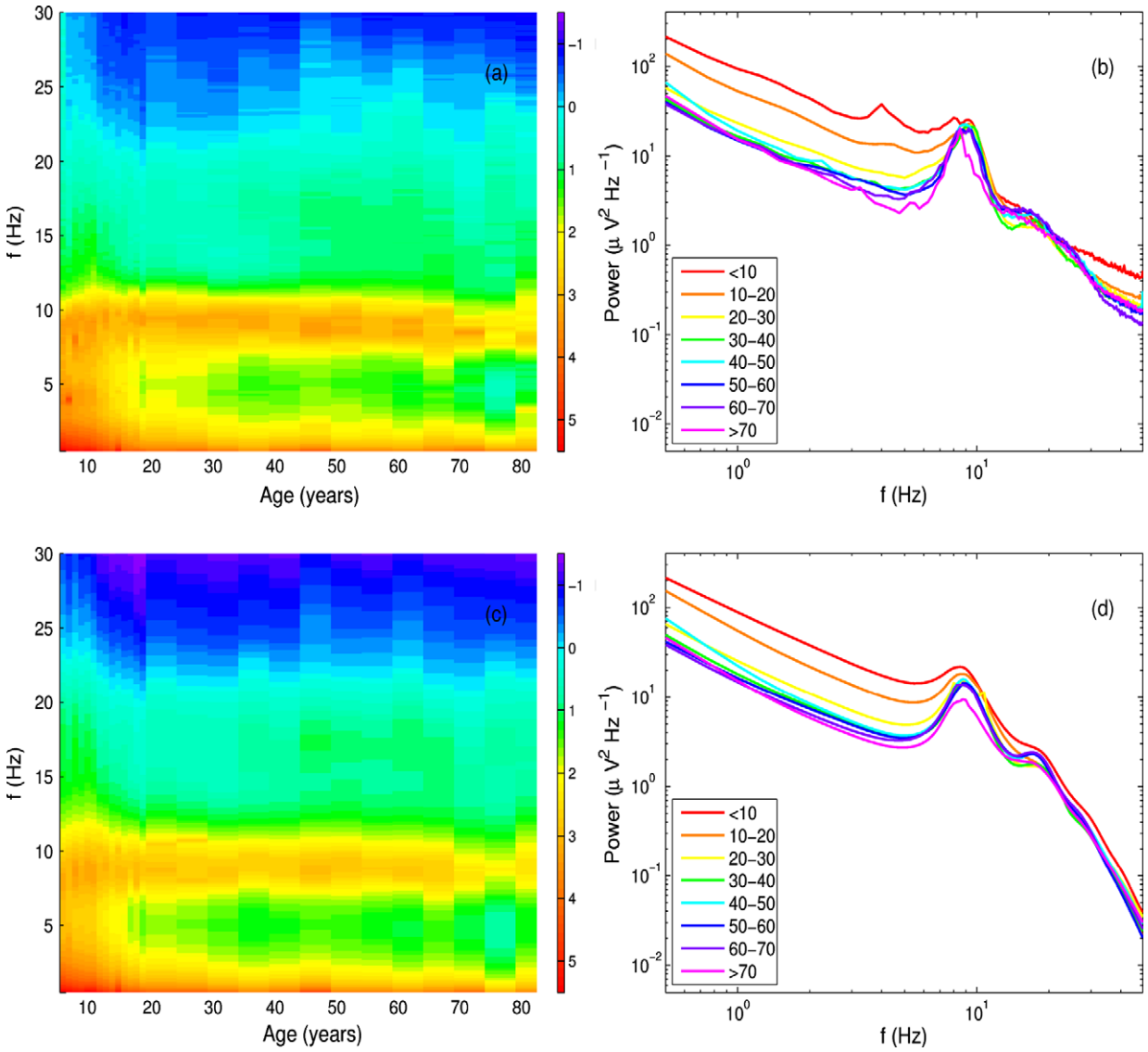

Fig. 9. Changes across age in empirical and fitted spectra. (a) Empirical spectral power averaged across individuals for frequencies up to 30 Hz; (b) double logarithmic plots of averaged empirical spectra; (c) and (d) corresponding plots for fitted spectra. The color bars indicate the logarithm of the dimensionless version of spectral power in $\mu V^2\ Hz^{-1}$, and the legends of (b) and (d) indicate age in years. The model spectra show a rapid fall-off at high frequencies because the fitted EMG component is not plotted.

4. Discussion

This study considered age trends in parameters obtained by model fits to empirical EEG spectra of a large sample (1498 subjects) of healthy males and females aged 6–86 years. Theoretical spectra were generated from a mean-field model of the thalamocortical system, describing interactions between excitatory and inhibitory cortical populations, and thalamic relay and reticular nuclei. Fitting to these spectra provided physiologically meaningful information on the neuronal substrates underlying the EEG. Fitted parameters were an average synaptodendritic decay rate (α), a damping rate for cortical propagating waves (γ), an average axonal delay for a full thalamocortical loop (t_0), an overall power normalization parameter (p_0), and gains for excitatory and inhibitory cortical interactions (G_{ee} and G_{ei}, respectively), a direct loop between cortex and relay nuclei (G_{ese}), an indirect thalamocortical loop passing through the reticular nucleus (G_{esre}), and an intrathalamic loop (G_{srs}). Net inhibitory connections or loops were represented by negative gains (G_{ei}, G_{esre}, and G_{srs}), whereas net excitatory interactions had positive gains (G_{ee} and G_{ese}). The robustness of fits was assessed by refitting empirical spectra with noise added, and comparing old and new parameter values.

Age trends were approximated by smooth asymptotically linear functions with a single turning point. In the literature, age trends for EEG parameters have been described using linear functions (e.g., (John et al., 1980; Matoušek et al., 1967; Polich, 1997), piecewise linear functions (e.g., (Duffy et al., 1993; Hughes and Cayaffa, 1977; Somsen et al., 1997), or polynomials (e.g., (Aurlien et al., 2004; Duffy et al., 1993). The functions proposed here have the advantage that (i) they are smooth and hence more physiologically realistic than piecewise linear functions; (ii) they are able to follow both fast trends during "development" and slower trends during "aging", unlike single linear functions; (iii) they have only four parameters (or five, including the characteristic age range over which slopes change considerably, which was fixed here), which have a simple interpretation in terms of asymptotic slopes and intercepts, in contrast to polynomial functions with variable numbers of parameters and no clear interpretation.

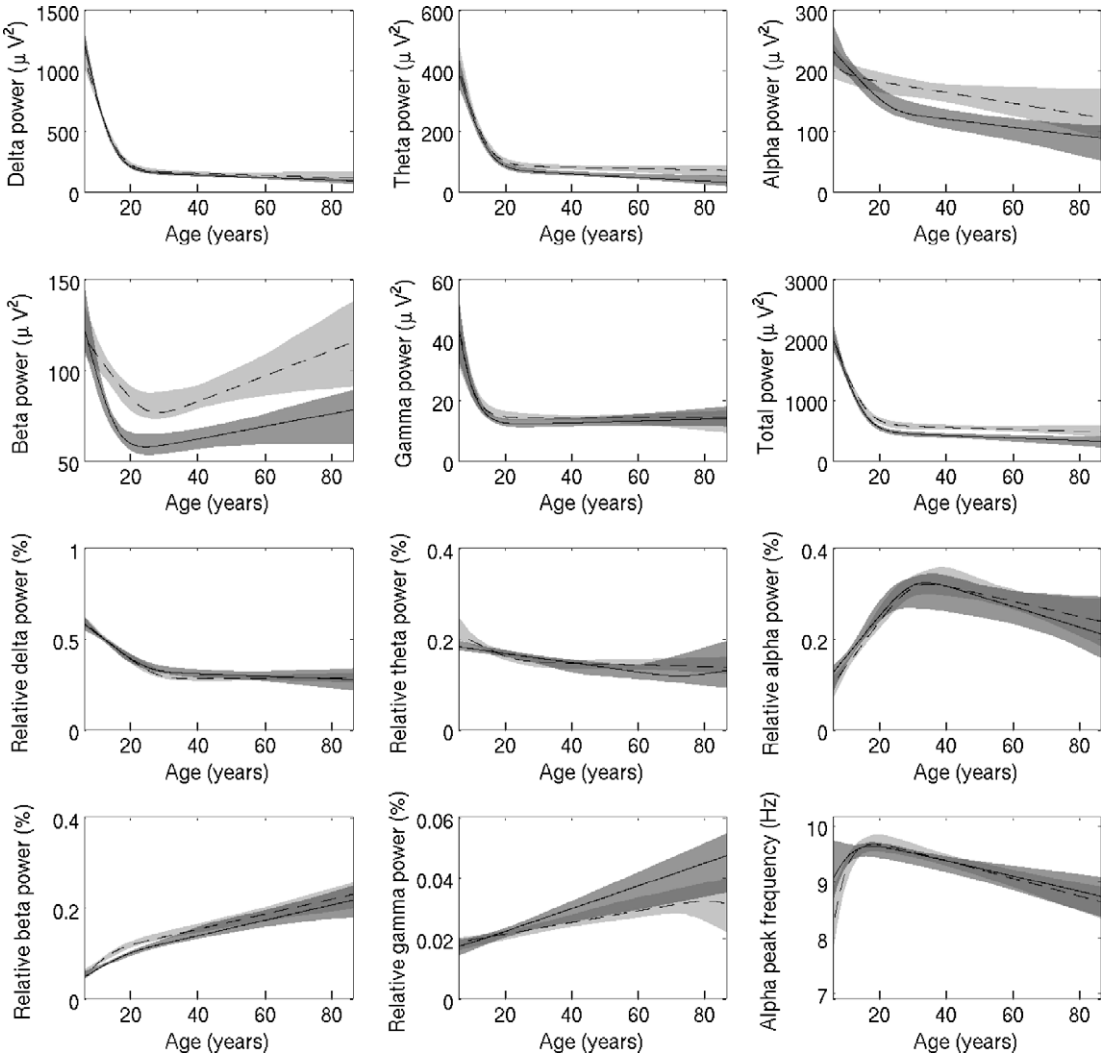

Fig. 10. Age trends in qEEG parameters determined using the functional form (2), with 95% confidence intervals. Solid lines, males; dashed lines, females.

Since EEG trends in the literature are often reported in terms of absolute and relative band powers and alpha peak frequencies, results on these quantitative EEG (qEEG) measures and their age trends were also presented. Furthermore, the relationships between model parameters and qEEG parameters were investigated. Aided by the large sample size, many significant results were found, which we summarize here and interpret in the light of the relevant literature. For each parameter, we first discuss

Table 5
Relationships between model parameters and qEEG parameters determined from model spectra. Model parameters were varied around their fitted values, and Spearman correlations were calculated between differences in model parameters and differences in qEEG parameters. Absolute values >0.050 for correlations were significant at the 0.05 level, those >0.065 at the 0.01 level, and those >0.085 at the 0.001 level. Significant correlations ($p < 0.05$) are shown in bold. Band limits were: delta, 0.5–4 Hz; theta, 4.25–8 Hz; alpha, 8.25–12 Hz; beta, 12.25–30 Hz; gamma: 30.25–49.5 Hz. Total power was calculated over the range 0.5–49.5 Hz. Alpha peak frequencies correspond to the frequencies where power was maximal in the range 5–13 Hz.

	$\Delta\alpha$	$\Delta\gamma$	Δt_0	ΔG_{ee}	ΔG_{ei}	ΔG_{ese}	ΔG_{esre}	ΔG_{srs}	Δp_0
Δ Power (μV^2)									
Δ Delta	0.0071	**0.098**	−0.025	**0.20**	**0.38**	**−0.15**	**−0.11**	**0.30**	**0.50**
Δ Theta	−0.011	**0.088**	**0.085**	**0.15**	**0.42**	−0.038	**0.068**	**0.21**	**0.63**
Δ Alpha	**0.19**	**0.24**	−0.0080	0.036	**0.50**	**0.13**	0.050	−0.027	**0.53**
Δ Beta	**0.37**	**0.26**	0.013	−0.024	**0.40**	−0.019	0.039	**−0.091**	**0.60**
Δ Gamma	**0.44**	**0.43**	0.015	−0.043	**0.29**	−0.017	0.033	**−0.055**	**0.50**
Δ Total	**0.11**	**0.18**	0.013	**0.14**	**0.47**	−0.037	−0.016	**0.16**	**0.58**
Δ Relative power (%)									
Δ Delta	**−0.23**	**−0.19**	**−0.090**	**0.24**	−0.046	**−0.28**	**−0.25**	**0.43**	−0.028
Δ Theta	**−0.29**	**−0.26**	**0.19**	0.0058	**−0.13**	0.0094	**0.23**	**0.060**	0.0078
Δ Alpha	**0.19**	**0.22**	−0.024	**−0.18**	**0.19**	**0.36**	**0.13**	**−0.33**	0.026
Δ Beta	**0.44**	**0.16**	0.026	**−0.25**	**−0.17**	−0.027	0.044	**−0.43**	0.020
Δ Gamma	**0.48**	**0.40**	−0.0083	**−0.20**	**−0.15**	−0.021	0.031	**−0.27**	0.012
Δ Alpha peak frequency (Hz)									
	0.44	**0.18**	**−0.27**	**−0.15**	−0.0069	−0.013	**−0.17**	**−0.30**	−0.022

significant sex differences when present, then summarize age trends, relate these trends to qEEG changes, and finally discuss possible relationships with physiological changes in childhood and adulthood.

4.1. General findings

The most robustly fitted parameter was G_{srs}, followed, respectively, by t_0, α, G_{ee}, p_0, G_{esre}, γ, and G_{ese}. We found the least robust parameter to be G_{ei}, consistent with the earlier result that this gain varied widely within individuals in a study of males aged 18–28 years (van Albada et al., 2007).

Between-fit differences in parameters were significantly correlated for a large number of parameter pairs. This occurs both because different sets of parameters can yield identical spectra, and because of the differential dependence of the goodness of fit on the parameters. The former introduces uncertainty in fitted parameters even if the spectrum is perfectly known, whereas the latter introduces additional uncertainty due to the presence of noise. Associations between parameters due to these effects may cause age trends that are not physiological in origin, so trends in parameters that are not highly robust should be interpreted with particular caution.

Averaged across age, there were significant sex differences in t_0, G_{ese}, G_{esre}, and G_{srs} : t_0 and $|G_{srs}|$ were larger in females, whereas G_{ese} and $|G_{esre}|$ were smaller. These sex differences were small compared to changes across the life span in either sex. Similarly, EEGs depended less on sex than on age in a study of a large group of healthy children and young adults (Matsuura et al., 1985). Average values of α, γ, G_{ee}, G_{ei}, and p_0 did not differ significantly between males and females. Although no significant sex difference in p_0 was found across age, trends in females clearly leveled off to higher values than in males during adulthood.

Parameter changes occurred most rapidly during childhood, and trends generally leveled off and sometimes reversed around adolescence. There were some sex differences in age trends besides those in p_0, which are more fully described below.

4.2. Synaptodendritic rate α

The average decay rate α for cell-body potentials in response to synaptic inputs, and by implication also the rise rate β (since $\beta = 4\alpha$ was imposed), decreased until about age 18, followed in males by a slight increase.

Smaller values of α enhance the low-pass filter properties of the synapses and dendrites, and correspond to less high-frequency ($\gtrsim 30$ Hz) activity in the EEG (Rowe et al., 2004). The relative constancy of α for adults in our study suggests that increases in relative high-frequency power with age in adulthood (Dustman et al., 1999) are largely independent of changes in synaptodendritic rates.

Several factors may contribute to the observed trends in α. First, a number of studies have found the total length of dendrites in the human cortex to increase in childhood, over longer periods in frontal than in visual areas (Becker et al., 1984; Huttenlocher, 1990), a process that may continue even into old age in some areas (Buell and Coleman, 1979, 1981). Unless the dendritic thickness increases proportionally to the square of the length, this is expected to increase the electrotonic length of neurons (Hill et al., 1994), leading to larger effective time constants (Ascoli, 2003). Unfortunately, investigations of dendritic thickness are sparse and rarely quantitative, at best allowing the conclusion that dendritic thickness of pyramidal neurons in certain cortical layers and areas increases slightly at least until age 5 years (Koenderink and Uylings, 1995; Petanjek et al., 2008).

Alterations in intrinsic membrane properties and numbers of neurotransmitter receptors are also expected to affect α. Expanded membrane surface and reduced capacitance have been suggested to contribute to decreases in membrane time constants during maturation (Tennigkeit et al., 1998; Warren and Jones, 1997), in contrast with the trend in α until age 18 found here (note that α is an inverse time constant). The expression of subunits of the NMDA receptor, which mediates slow glutamatergic transmission, reaches a peak in early development, after which it declines at a decreasing rate (Magnusson et al., 2002; Ontl et al., 2004). This decline is also expected to increase α.

A number of studies have reported shrinkage of the dendritic trees of some neuronal types in adulthood (de Brabander et al., 1998; Esiri, 2007; Jacobs et al., 1997; Uylings and de Brabander, 2002), which may contribute to slight increases in α in this age range. On the other hand, Luebke and Rosene (2003) reported significantly longer decay times of inhibitory postsynaptic currents in hippocampal cells of aged compared to young monkeys. This was tentatively attributed to changes in the subunit composition of $GABA_A$ receptors, as found by Gutiérrez et al. (1997) in rat cerebellum and cerebral cortex. These effects would tend to decrease α, and thus cannot account for the trends in adults seen in our study. Therefore, these results merit further investigation.

4.3. Cortical damping rate γ

A damped-wave equation for cortical activity was included in the model based on experimental observations of spreading waves of neuronal activity in response to localized stimulation (Chervin et al., 1988; Nunez, 1974; Schiff et al., 2007; Xu et al., 2007). The parameter γ, representing the characteristic damping rate of such waves, increased in both sexes until about age 20, after which the trends leveled off, and even reversed in females.

Larger values of γ are associated with sharper, larger-amplitude, and slightly higher-frequency peaks in the EEG spectrum (Rowe et al., 2004). Thus, changes in the damping rate of cortical waves may contribute to the shift of alpha peaks to higher frequencies during childhood (Hughes, 1987; Kooi, 1971; Niedermeyer, 1982; Somsen et al., 1997), and the narrowing of alpha peaks that was found by Alvarez Amador et al. (1989) at the C3 electrode. Power augmentation due to larger γ was offset by other parameter changes, including reduced p_0 (see below), to yield a net decline in peak amplitudes, in agreement with the literature (Niedermeyer, 1982).

Since γ is the ratio of the average axonal propagation speed and the typical range of cortical pyramidal axons, increased γ is associated with faster transmission and/or shorter effective ranges (although the characteristic range of pyramidal axons was fixed in this study). Ongoing cortical myelination (Perrin et al., 2008; Sowell et al., 2003) may contribute to increases in γ throughout childhood and adolescence by increasing axonal transmission speeds. However, the more rapid growth of white matter in boys than in girls (Caviness et al., 1996; De Bellis et al., 2001; Perrin et al., 2008) did not translate into greater slopes for γ in our study.

A number of studies have found reductions in white matter volume during aging, especially from the fifth decade onward (Ge et al., 2002; Miller et al., 1980; Piguet et al., 2009). Even in myelin sheaths that continue to grow during aging, defects accumulate, and thick sheaths are prone to splitting (Peters, 2002a; Peters, 2002b). Myelin defects reduce conduction velocities along nerve fibers (Felts et al., 1997; Gutiérrez et al., 1995; Xi et al., 1999). These effects may have contributed to decreases in damping rates in women.

4.4. Corticothalamic loop delay t_0

Averaged across the entire age span, the axonal delay t_0 was slightly longer in females than in males. This delay depends on the distance between cortex and thalamus, and velocities along corticothalamic and thalamocortical fibers. Since females have smaller brains on average (Caviness et al., 1996; Dekaban and

Sadowsky, 1978), our finding suggests that the propagation speed along axons is more than proportionately smaller in females. This may be related to the smaller percentage of white matter in female compared to male brains (Cosgrove et al., 2007). Since the location of the alpha peak in model spectra depends on the inverse of t_0, this is expected to correspond to higher alpha peak frequencies in males than in females. Males did consistently show slightly higher peak frequencies across age and sites, except around age 20, when females had higher peak frequencies (not shown). Averaged across age, we did not find significant sex differences in alpha peak frequencies at the Cz electrode.

Our results contrast with the finding that alpha peak frequencies are on average slightly higher in females than in males up to age 12–13 (Petersén and Eeg-Olofsson, 1971), as well as averaged over the entire life span (Aurlien et al., 2004). This discrepancy may be partly explained by the fact that neither Petersén and Eeg-Olofsson (1971) nor Aurlien et al. (2004) used spectral analysis, and instead relied on time series (which leads to less precise estimates, particularly since traces are modulated by lower-frequency activity). Furthermore, Aurlien et al. studied patients with various pathologies (mostly epilepsy), and selected the highest alpha frequency for each subject. All these factors make it difficult to compare their findings with ours.

The decline in t_0 observed in males up to age ~15, and in females up to age ~20, parallelled accelerated alpha rhythms. This corresponds well with findings reported in the literature, as summarized for instance by Petersén et al. (1975) and Klimesch (1999). An increase in the frequency of the alpha peak from about 5–6 Hz to 10 Hz is observed in children between ages 1 and 15 years (Hughes, 1987; Kooi, 1971; Niedermeyer, 1982; Somsen et al., 1997). Our data appear to confirm the finding by Petersén and Eeg-Olofsson (1971) that the alpha rhythm increased in frequency faster in girls than in boys. However, white matter volume has been reported to increase faster in boys than in girls after age 6 (Caviness et al., 1996; De Bellis et al., 2001; Perrin et al., 2008), in agreement with more marked reductions in t_0 in boys found here. This suggests that developmental changes in alpha peak frequencies depend not only on white matter growth, but also on other factors. Our results show less marked reductions in synaptodendritic rates in girls than in boys, as well as greater increases in the interaction strength between the thalamic relay and reticular nuclei ($|G_{srs}|$); both tend to enhance increases in alpha peak frequency.

In both sexes t_0 increased into old age, associated with a gradual reduction in the frequency of the alpha peak. These trends may be linked to loss of white matter and accumulating damage to myelin sheaths in adulthood (Peters, 2002a,b; Piguet et al., 2009). Decreased alpha peak frequencies are consistent with some early studies of aged individuals without organic brain disease (Hughes and Cayaffa, 1977; Obrist, 1954), but were either not found in more tightly controlled samples, or attributed to age-related pathologies (Duffy et al., 1984; Duffy et al., 1993; Katz and Horowitz, 1982). However, Klimesch (1999) noted that the absence of a significant trend in alpha peak frequency reported by Duffy et al. (1984) was due to a relative lack of change between 30 and 50 years, whereas this frequency diminished by about 1 Hz between the ages of 60 and 80. We also observe that slight decreases in the frequency of the alpha peak may not have reached statistical significance due to the relatively small sample (63 subjects) used by Duffy et al. (1984). In agreement with our results, Aurlien et al. (2004) found dominant alpha frequencies to decrease after age 45.

4.5. Gains

All gains except that for the loop between thalamic relay and reticular nuclei, G_{srs}, had larger average absolute values in males. More negative G_{srs} corresponds to differences in qEEG measures including greater absolute and relative beta power. Thus, the greater absolute and relative beta power in women than in men found here and reported in the literature (Veldhuizen et al., 1993) may be related to stronger interactions between the thalamic relay and reticular nuclei in women.

On average, the absolute values of all gains except G_{srs} diminished with age. The cortical excitatory gain G_{ee} decreased in childhood in both males and females, after which it increased in males but stayed about constant in females. The greatest reduction in the cortical inhibitory gain $|G_{ei}|$ occurred up to age ~20, and trends in both sexes leveled off thereafter. Boys and girls showed opposite trends in the corticothalamic loop gain G_{ese}, which decreased in the former but increased in the latter. The trend for females reversed around age 40. The gain for the corticothalamic loop passing through the thalamic reticular nucleus, $|G_{esre}|$, decreased mostly at young ages in males, but mostly during old age in females.

Relative delta and theta power gradually diminished during childhood, as also reported in the literature (Alvarez Amador et al., 1989). Sensitivity analysis suggested that stronger interactions between the thalamic relay and reticular nuclei (quantified by G_{srs}) contribute to reductions in relative low-frequency power and increases in relative beta and gamma power. Reductions in G_{ee} tend to decrease relative delta power and increase relative beta and gamma power, while reductions in $|G_{ei}|$ decrease relative theta power. Increases in G_{ese} in girls, and decreases in $|G_{esre}|$ in boys, may contribute to reductions in relative delta power.

Reductions in G_{ee} may have a variety of causes. Extensive pruning of excitatory synapses occurs in primate cortex during adolescence (Gonzalez-Burgos et al., 2008). The density of NMDA glutamate receptors decreases with age, and reduced cortical glutamate content has been observed in aged animals (Segovia et al., 2001). Although decreased glutamate uptake may compensate partly for the decline in glutamate release, these findings appear to support a reduction in G_{ee}. It is particularly striking that G_{ee} decreases until about age 40, found by Jacobs et al. (1997) to be the age at which dendritic spine numbers in two cortical areas approximately stabilize after marked reductions. These findings do not explain the observed sex differences in trends in G_{ee}, so this issue deserves further exploration.

The observed decline in $|G_{ei}|$ during childhood is surprising, since the number of GABAergic synapses increases in this period of life (Heinen et al., 2003), and the brain becomes less vulnerable to epileptic seizures (Camfield et al., 1996). Furthermore, Luebke et al. (2004) found synaptic inhibition in the monkey prefrontal cortex to increase with age. On the other hand, the open times of $GABA_A$ receptors shorten during development, impairing inhibitory synaptic transmission (Bosman et al., 2005). There is some experimental evidence supporting the reduction in inhibitory cortical interactions in adulthood found here. Poe et al. (2001) described an age-related reduction in the numbers of putative inhibitory synapses in layer 2 of rat somatosensory cortex. Furthermore, some studies with transcranial magnetic stimulation have revealed reduced excitability of cortical inhibitory circuits with aging (Hortobágyi et al., 2006; Peinemann et al., 2001).

Early increases in $|G_{srs}|$ may be related to the growing ability of reticular neurons to sustain bursts of activity (Tennigkeit et al., 1998; Warren and Jones, 1997). In addition, substantial growth of dendritic arbors occurs during maturation (Warren and Jones, 1997), possibly enabling more synaptic contacts to be established. However, dendritic growth cannot account for continued increases in $|G_{srs}|$ during adulthood, which is characterized by regressive processes (Abe et al., 2008). Enhanced expression of metabotropic glutamate receptors in the thalamus during aging (Simonyi et al., 2005) may play a role in the observed trends in G_{srs}. Loss of synapses may explain the significant reductions in G_{ese} and $|G_{esre}|$ in adults found here.

4.6. Spectral power normalization p_0

We found that the power normalization parameter p_0 was slightly larger on average in females than in males, although this difference was not significant at the 0.05 level. This accords with the finding that the skulls of white males are slightly thicker at the vertex throughout life than those of white females (Adeloye et al., 1975), since thicker skulls cause greater attenuation of the signal. However, no such differences were found in black subjects, and females had thicker skulls than males at parietal and parieto-occipital sites in the third decade and after age 60. Thus, different findings for p_0 may be expected at electrode sites other than Cz.

The parameter p_0 diminished until age $\sim$20, after which it showed a slower decrease that was slightly more pronounced in males. The negative trend in p_0 agrees with the decrease in EEG amplitude with age found here and reported in the literature (Aurlien et al., 2004; Hartikainen et al., 1992; Matoušek et al., 1967; Polich, 1997). EEG amplitude has been reported to increase until 6–11 years and then diminish (Hughes, 1987; Petersén and Eeg-Olofsson, 1971; Petersén et al., 1975). Similarly, closer inspection of our data revealed that p_0 only decreased systematically from about age 10 onward. Due to the relatively small number of subjects aged >80 years, it was not possible to verify from our data if power increased again in the very old, as reported by Aurlien et al. (2004).

Increases in skull thickness in the first two decades of life (Adeloye et al., 1975) may account for substantial decreases in EEG power recorded on the scalp (Eshel et al., 1995). The reduction in brain volume across the life span is also likely to be linked to negative trends in p_0. Most studies find that age-related atrophy is more extensive in men than in women (Coffey et al., 1998; Cowell et al., 1994; Gur et al., 1991; Tomlinson et al., 1968; Xu et al., 2000), although the onset may be earlier in women (Hatazawa et al., 1982; Hubbard and Anderson, 1983). Greater changes in peripheral and lateral fissure cerebrospinal fluid volume were also observed in men than in women between 65 and 95 years of age (Coffey et al., 1998). These results accord with the steeper slope in p_0 for males compared to females aged $\gtrsim 20$ in our study, although the difference in age correlations was not statistically significant. Reductions in total power across the life span were also slightly greater in men than in women.

4.7. Outlook

This study has shown that mean-field modeling of brain electrical activity presents a viable alternative to classical qEEG, enabling physiological information to be extracted from EEG spectra. The large number of subjects (1498) allowed reliable estimation of average age trends, even with large inter-individual scatter. The average parameter values for healthy individuals across age provide a standard against which clinical groups may be compared.

The model parameters describe large-scale properties of the brain, and as such provide different information than that afforded by most invasive techniques. Moreover, the connection with physiology is an advantage over many other noninvasive techniques. Furthermore, model spectra match most features of empirical spectra, and thus capture most of the information present in absolute and relative band powers and alpha peak frequencies, but contain additional information about spectral shape within bands. Thus, the method presented allows questions about age-related changes in the properties of the brain to be answered that are not readily addressed using other methods.

The cross-sectional design has the potential disadvantage that the results are affected by differences across generations, for instance due to changes in nutrition or education. However, a longitudinal study of the age range considered here would take at least 80 years to complete, rendering this approach highly impractical.

Parallels between age trends in fitted model parameters and known physiological trends provide evidence that the physiological interpretations made of model parameters are plausible. For instance, decreases followed by increases in axonal delays accord with white matter growth during childhood and subsequent accumulation of myelin defects. Similarly, acceleration of axonal conduction due to myelination may account for increases in the damping rate of cortical waves during development. Furthermore, reductions in absolute gain values plausibly reflect synaptic pruning processes. However, there are also discrepancies between parameter trends and known physiological changes. For instance, a number of empirical studies suggest increases followed by decreases in synaptodendritic rates, opposite to our findings. It is hoped that the comparisons presented here will help to spur on further development of realistic models of EEG generation.

An identical subject set will be used to compare our results with data on alpha peak morphology (Chiang et al., 2008), model fits to EPs (Kerr et al., 2008), and EP deconvolution parameters (Kerr et al., 2009), eliminating important sources of experimental bias and uncertainty. It would also be desirable to compare the Cz data presented here with data from other electrodes, to assess differences in aging processes across brain regions. In addition, it will be possible to determine links with genetics and measures of general and social cognition using data from the Brain Resource International Database (www.brainresource.com) (Gordon et al., 2005). Great advantages of this standardized database are its size, diversity of recording modalities, and the uniformity of exclusion criteria and experimental conditions. Convergent evidence from different modalities will help to elucidate some of the links between the physiological substrates and functional aspects of brain aging.

Acknowledgements

We acknowledge the support of the Brain Resource International Database (under the auspices of Brain Resource; www.brainresource.com) for data acquisition and processing. All scientific decisions are made independently of any BR commercial decisions via the independently operated scientific division, BRAINnet (www.brainnet.net), which is overseen by the Brain Dynamics Centre and scientist members. We thank the individuals who gave their time to take part in the study. This work was supported by an Endeavour International Postgraduate Research Scholarship, an International Postgraduate Award, and the Australian Research Council.

Appendix A

A.1. Mathematical description of model

With each neuronal population we associate a pulse rate field, which is a continuum estimate of the average rate of incoming action potentials for that population. The pulse rate field is denoted $\phi_a(\mathbf{r},t)$, where $\mathbf{r}$ is a spatial coordinate within each neuronal population, and the subscript a represents the relevant population. For a given receiving population, the contributions of all afferent populations are weighted by the relevant connection strengths and summed. Dendritic and synaptic delays are modeled using a second-order differential equation that incorporates characteristic rise and decay rates of the membrane potential, respectively denoted β and α. The equations for dendritic and synaptic summation and integration are then (Robinson et al., 1997, 2002)

$$D_{\alpha\beta}(t)V_a(\mathbf{r},t)=\sum_b v_{ab}\phi_b(\mathbf{r},t-\tau_{ab}), \tag{5}$$

$$D_{\alpha\beta}(t)=\frac{1}{\alpha\beta}\frac{d^2}{dt^2}+\left(\frac{1}{\alpha}+\frac{1}{\beta}\right)\frac{d}{dt}+1, \tag{6}$$

where V_a is the average cell-body potential of population a, $v_{ab} = N_{ab}s_b$ are connection strengths consisting of the unitary synaptic strength s_b and the number of synapses N_{ab} from neurons of type b per type a neuron, and τ_{ab} is the relevant axonal delay. The axonal delay for a full loop between cortex and thalamus is denoted t_0. The total delay necessary to complete a corticothalamic loop depends also on dendritic and synaptic integration times, and is slightly longer than t_0. In our model, the inverse of this total delay determines the location of the alpha peak in the frequency spectrum (Robinson et al., 2002).

When fitting to empirical spectra, a reduction in the number of independent parameters is achieved by setting $\alpha = \beta/4$, which agrees roughly with experimental results (Rowe et al., 2004). The number of fitted parameters is further reduced using the proportionality of the total number of synapses between two populations to the numbers of sending and receiving neurons, which holds approximately in the cortex (Braitenberg and Schüz, 1998; Robinson et al., 2001a; Wright and Liley, 1995). Hence, the number of synapses *per cortical neuron* depends only on the afferent population, implying $N_{eb} = N_{ib}$ and $G_{eb} = G_{ib}$ for $b = e, i, s$ (note that we have approximated unitary synaptic strengths s_b as depending only on the sending population).

The outgoing firing rate field depends on the cell-body potential via a sigmoidal function, which results from the contribution of neurons with different firing thresholds. We use (Robinson et al., 1997, 1998, 2001a, 2003),

$$Q_a(\mathbf{r},t) = S[V_a(\mathbf{r},t)] = \frac{Q_{\max}}{1+\exp[-(V_a-\theta)/\sigma']}, \tag{7}$$

where $Q_{\max}$ is the maximum firing rate, θ is the average threshold potential, and $\sigma'\pi/\sqrt{3}$ is the standard deviation of firing thresholds (Wright and Liley, 1995). The version of the model used in the present study imposes equal values of $Q_{\max}$, θ, and σ' for all components, which may be interpreted as average or effective values.

The cortex is modeled as a two-dimensional sheet (parameterized by $\mathbf{r}$) owing to its relative thinness. Many experimental studies have shown that localized cortical stimulation leads to waves of neuronal activity spreading across the cortex (Chervin et al., 1988; Nunez, 1974; Schiff et al., 2007; Xu et al., 2007), a feature included in a number of earlier models (Beurle, 1956; Bressloff, 2001; Bressloff et al., 2003; Jirsa and Haken, 1996; Jirsa and Haken, 1997; Nunez, 1995). We use a damped-wave equation for the excitatory pulse rate field (Robinson et al., 1997; Robinson et al., 1998; Robinson et al., 2001a; Robinson et al., 2003),

$$\left[\frac{1}{\gamma^2}\frac{\partial^2}{\partial t^2} + \frac{2}{\gamma}\frac{\partial}{\partial t} + 1 - r_e^2\nabla^2\right]\phi_e(\mathbf{r},t) = Q_e(\mathbf{r},t), \tag{8}$$

where isotropy and homogeneity have been assumed, r_e is the characteristic range of pyramidal axons, $\gamma = v_e/r_e$ is the damping rate of cortical waves, and v_e represents the axonal propagation speed. The typical range of axons within the remaining populations is taken to be short enough to ignore wave propagation effects, allowing us to set $\phi_a(\mathbf{r},t) = Q_a(\mathbf{r},t)$ for $a = i, s, r$, which has been termed the local activity approximation (Robinson et al., 2004). The signals from these populations therefore influence their targets via delayed one-to-one mappings.

Setting the spatial and temporal derivatives in Eqs. (5) and (8) to zero yields an odd number of uniform fixed points $\phi_a^{(0)} = Q_a^{(0)}$, usually one or three (Robinson et al., 2002). Stable fixed points represent steady states to which the system settles down unless perturbed. For physiological parameters we expect a low-firing-rate steady state, around which small perturbations can be described using a linear approximation,

$$Q_a(\mathbf{r},t) = Q_a^{(0)} + \rho_a\left[V_a(\mathbf{r},t) - V_a^{(0)}\right], \tag{9}$$

$$\rho_a = \left.\frac{dQ_a(\mathbf{r},t)}{dV_a(\mathbf{r},t)}\right|_{V_a^{(0)}}, \tag{10}$$

$$= \frac{Q_a^{(0)}}{\sigma'}\left[1 - \frac{Q_a^{(0)}}{Q_{\max}}\right], \tag{11}$$

where $V_a^{(0)}$ is the steady-state value of the mean membrane potential (Robinson et al., 2004), and ρ is the derivative of the sigmoid at steady state. Henceforth denoting $V_a - V_a^{(0)}$ simply by V_a, and similarly for Q_a and ϕ_a, Fourier transformation of Eqs. (5), (8), and (9) yields (Robinson et al., 2001a)

$$Q_a(\mathbf{k},\omega) = \rho_a V_a(\mathbf{k},\omega), \tag{12}$$

$$= L(\omega)\sum_b G_{ab}\phi_b(\mathbf{k},\omega)e^{i\omega\tau_{ab}}, \tag{13}$$

$$= \begin{cases} \left[\left(1-\frac{i\omega}{\gamma}\right)^2 + \frac{k^2 v_e^2}{\gamma^2}\right]\phi_e(\mathbf{k},\omega) \\ \quad \text{(cortical excitatory neurons)}, \\ \phi_a(\mathbf{k},\omega) \\ \quad \text{(all other populations)}, \end{cases} \tag{14}$$

where

$$L(\omega) = \left(1-\frac{i\omega}{\alpha}\right)^{-1}\left(1-\frac{i\omega}{\beta}\right)^{-1}. \tag{15}$$

Here, $\mathbf{k}$ and ω denote wavenumbers and angular frequencies, and $G_{ab} = \rho_a v_{ab}$ are linear gains representing the number of additional pulses out per additional pulse in. Eqs. (13) and (14) allow us to derive a linear transfer function $\phi_e(\mathbf{k},\omega)/\phi_n(\mathbf{k},\omega)$ describing the cortical response to input from underlying structures. For the neuronal connections in Fig. 2, the transfer function is (Robinson et al., 2002, 2004)

$$\frac{\phi_e(\mathbf{k},\omega)}{\phi_n(\mathbf{k},\omega)} \equiv T(\mathbf{k},\omega) = \frac{1}{(k^2+q^2)r_e^2}\frac{G_{es}G_{sn}L^2 e^{i\omega t_0/2}}{(1-G_{srs}L^2)(1-G_{ei}L)}, \tag{16}$$

$$q^2 r_e^2 = \left(1-\frac{i\omega}{\gamma}\right)^2 - \frac{L}{1-G_{ei}L}\left[G_{ee} + \frac{(G_{ese}L + G_{esre}L^2)e^{i\omega t_0}}{1-G_{srs}L^2}\right], \tag{17}$$

where we have defined $G_{ese} = G_{es}G_{se}$ for the direct corticothalamic loop, $G_{esre} = G_{es}G_{sr}G_{re}$ for the indirect corticothalamic loop passing through the reticular nucleus, and $G_{srs} = G_{sr}G_{rs}$ for the intrathalamic loop between relay nuclei and the reticular nucleus. We see that the cortical signal depends only on these gain products, which can be interpreted as being distributed around loops rather than localized to single populations.

A.2. Frequency spectra

The EEG is the result of dendritic and synaptic currents of many cortical neurons firing in partial synchrony (Nunez, 1995; Ray, 1990). Excitatory pyramidal neurons are the largest and most aligned among cortical neuronal types, and are thus expected to dominate the signal (Nunez, 1995; Robinson et al., 2001a). Furthermore, the EEG is thought to depend much more strongly on excitatory synaptic input to apical dendrites of pyramidal cells than on inhibitory input to basal dendrites. One reason for this is that the basal dendrites are closer to the relatively conductive cell body, causing dipoles to arise only over small distances. In addition, basal dendrites are less aligned than apical dendrites, and their synaptic actions are less layer-specific (Mitzdorf, 1985; Towe, 1966). We can therefore approximate the dendritic and synaptic currents responsible for EEG fluctuations as being roughly proportional to the pulse rate field ϕ_e.

The frequency spectrum measured on the scalp is a low-pass filtered version of that on the cortical surface, due to volume conduction attenuating the large-wavenumber content of the signal, and the association of large wavenumbers with high frequencies. Furthermore, the signal measured on the scalp contains a contribution from the muscles. For the purpose of model fitting, input from underlying structures is approximated as spatiotemporal white noise, represented by a constant modulus and random phase in the Fourier domain, $|\phi_n(\mathbf{k},\omega)|^2 = |\phi_n|^2$. This is consistent with evidence that EEG activity often has the properties of filtered noise (Lopes da Silva et al., 1974; Stam et al., 1999), and has proven to yield realistic spectra in previous works (Robinson et al., 2001a, 2003). Although boundary conditions have only small effects on the cortical spectrum (Robinson et al., 2001b), they were found to improve fits in some cases (Rowe et al., 2004). For a two-dimensional rectangular cortex of size $L_x \times L_y$, the spectrum can be written as a sum over a discrete set of wavenumbers taking the form (Rennie et al., 2002; Rowe et al., 2004; van Albada et al., 2007)

$$P_{the}(\omega) = P_{EEG}(\omega) + P_{EMG}(\omega), \tag{18}$$

$$P_{EEG}(\omega) = \frac{\pi|\phi_n|^2}{r_e^2} G_{es}^2 G_{sn}^2 \left| \frac{L^2 e^{i\omega t_0/2}}{(1-G_{srs}L^2)(1-G_{ei}L)} \right|^2 \mathscr{P} \tag{19}$$

$$\equiv 10^{p_0} \left| \frac{L^2 e^{i\omega t_0/2}}{(1-G_{srs}L^2)(1-G_{ei}L)} \right|^2 \mathscr{P}, \tag{20}$$

$$\mathscr{P} = \frac{4\pi r_e^2}{L_x L_y} \times \sum_{m,n=-M,-N}^{M,N} \frac{e^{-k_{mn}^2/k_0^2}}{|k_{mn}^2 r_e^2 + q^2 r_e^2|^2}, \tag{21}$$

$$P_{EMG}(\omega) = A_{EMG} \frac{(\omega/\omega_{EMG})^2}{[1+(\omega/\omega_{EMG})^2]^2}, \tag{22}$$

where the theoretical spectrum $P_{the}(\omega)$, which is a sum of EEG and electromyographic (EMG) components, is matched to the empirical spectrum via $1\ \mu V^2\ Hz^{-1}\ m^{-2} \equiv 1$. Furthermore, k_0 is a cut-off wavenumber for filtering by cerebrospinal fluid, skull, and scalp, which is taken into account via $\exp[-k_{mn}^2/k_0^2]$, and the discrete wavenumbers are given by

$$\mathbf{k}_{mn} = \left(\frac{2\pi m}{L_x}, \frac{2\pi n}{L_y}\right). \tag{23}$$

The EMG component has a maximum of $A_{EMG}/4$ at ω_{EMG}, taken to be $2\pi\times$ (40 Hz). The amplitude A_{EMG} is determined along with the other model parameters, but is not further considered here since we are interested in the activity of the brain itself. The parameter p_0 appearing in Eq. (20) provides a normalization for the spectrum without affecting its shape.

References

Abe O, Yamasue H, Aoki S, Suga M, Yamada H, Kasai K, et al. Aging in the CNS: comparison of gray/white matter volume and diffusion tensor data. Neurobiol Aging 2008;29:102–16.

Adeloye A, Kattan KR, Silverman FN. Thickness of the normal skull in the American blacks and whites. Am J Phys Antropol 1975;43:23–30.

Alvarez Amador A, Valdés Sosa PA, Pascual Marqui RD, Galan Garcia L, Biscay Lirio R, Bosch Bayard J. On the structure of EEG development. Electroencephalogr Clin Neurophysiol 1989;73:10–9.

Ascoli GA. Electrotonic effects on spike response model dynamics. IEEE Neural Networks 2003;4:2831–6.

Aurlien H, Gjerde IO, Aarseth JH, Eldøen G, Karlsen B, Skeidsvoll H, et al. EEG background activity described by a large computerized database. Clin Neurophysiol 2004;115:665–73.

Barnea-Goraly N, Menon V, Eckert M, Tamm L, Bammer R, Karchemskiy A, et al. White matter development during childhood and adolescence: a cross-sectional diffusion tensor imaging study. Cereb Cortex 2005;15:1848–54.

Becker LE, Armstrong DL, Chan F, Wood MM. Dendritic development in human occipital cortical neurons. Dev Brain Res 1984;13:117–24.

Beurle RL. Properties of a mass of cells capable of regenerating pulses. Phil Trans R Soc Lond B 1956;240:55–94.

Bosman LWJ, Heinen K, Spijker S, Brussaard AB. Mice lacking the major adult $GABA_A$ receptor subtype have normal number of synapses, but retain juvenile IPSC kinetics until adulthood. J Neurophysiol 2005;94:338–46.

Braitenberg V, Schüz A. Cortex: statistics and geometry of neuronal connectivity. 2nd ed. Berlin: Springer; 1998.

Breakspear M, Roberts JA, Terry JR, Rodrigues S, Mahant N, Robinson PA. A unifying explanation of primary generalized seizures through nonlinear brain modeling and bifurcation analysis. Cereb Cortex 2006;16:1296–313.

Bressloff PC. Traveling fronts and wave propagation failure in an inhomogeneous neural network. Physica D 2001;155:83–100.

Bressloff PC, Folias SE, Prat A, Li Y-X. Oscillatory waves in inhomogeneous neural media. Phys Rev Lett 2003;91:178101.1–1.4.

Buell SJ, Coleman PD. Dendritic growth in the aged human brain and failure of growth in senile dementia. Science 1979;206:854–6.

Buell SJ, Coleman PD. Quantitative evidence for selective dendritic growth in normal human aging but not in senile dementia. Brain Res 1981;214:23–41.

Camfield CS, Camfield PR, Gordon K, Wirrell E, Dooley JM. Incidence of epilepsy in childhood and adolescence: a population-based study in Nova Scotia from 1977 to 1985. Epilepsia 1996;37:19–23.

Caviness Jr VS, Kennedy DN, Richelme C, Rademacher J, Filipek PA. The human brain age 7–11 years: a volumetric analysis based on magnetic resonance images. Cereb Cortex 1996;6:726–36.

Chervin RD, Pierce PA, Connors BW. Periodicity and directionality in the propagation of epileptiform discharges across neocortex. J Neurophysiol 1988;60:1695–713.

Chiang AKI, Rennie CJ, Robinson PA, Roberts JA, Rigozzi MK, Whitehouse RW, et al. Automated characterization of multiple alpha peaks in multi-site electroencephalograms. J Neurosci Meth 2008;168:396–411.

Chiang AKI, Rennie CJ, Robinson PA, van Albada SJ. Age trends and sex differences of the alpha rhythm. in preparation.

Coffey C, Lucke J, Saxton J, Ratcliff G, Unitas L, Billig B, et al. Sex differences in brain aging. Arch Neurol 1998;55:169–79.

Cosgrove K, Mazure C, Staley J. Evolving knowledge of sex differences in brain structure, function, and chemistry. Biol Psychiatry 2007;62:847–55.

Cowell P, Turetsky B, Gur R, Grossman R, Shtasel D, Gur R. Sex differences in aging of the human frontal and temporal lobes. J Neurosci 1994;14:4748–55.

De Bellis M, Keshavan M, Beers S, Hall J, Frustaci K, Masalehdan A, et al. Sex differences in brain maturation during childhood and adolescence. Cereb Cortex 2001;11:552–7.

de Brabander JM, Kramers RJK, Uylings HBM. Layer-specific dendritic regression of pyramidal cells with ageing in the human prefrontal cortex. Eur J Neurosci 1998;10:1261–9.

Dekaban AS. Tables of cranial and orbital measurements, cranial volume, and derived indexes in males and females from 7 days to 20 years of age. Ann Neurol 1977;2:485–91.

Dekaban A, Sadowsky D. Changes in brain weights during the span of human life: relation of brain weights to body heights and body weights. Ann Neurol 1978;4:345–56.

Duffy FH, Albert MS, McAnulty G, Garvey AJ. Age-related differences in brain electrical activity of healthy subjects. Ann Neurol 1984;16:430–8.

Duffy FH, McAnulty GB, Albert MS. The pattern of age-related differences in electrophysiological activity of healthy males and females. Neurobiol Aging 1993;14:73–84.

Dustman RE, Shearer DE, Emmerson RY. Life-span changes in EEG spectral amplitude, amplitude variability and mean frequency. Clin Neurophysiol 1999;110:1399–409.

Eichorn DH, Bayley N. Growth in head circumference from birth through young adulthood. Child Dev 1962;33:257–71.

Eshel Y, Witman S, Rosenfeld M, Abboud S. Correlation between skull thickness asymmetry and scalp potential estimated by a numerical model of the head. IEEE Biomed Eng 1995;42:242–9.

Esiri MM. Ageing and the brain. J Pathol 2007;211:181–7.

Felts PA, Baker TA, Smith KJ. Conduction along segmentally demyelinated mammalian central axons. J Neurosci 1997;17:7267–77.

Gallagher M, Colombo P. Ageing: the cholinergic hypothesis of cognitive decline. Curr Opin Neurobiol 1995;5:161–8.

Gasser T, B acher P, Steinberg H. Test–retest reliability of spectral parameters of the EEG. Electroencephalogr Clin Neurophysiol 1985;60:312–9.

Gasser T, Verleger R, B acher P, Sroka L. Development of the EEG of school-age children and adolescents. I. Analysis of band power. Electroencephalogr Clin Neurophysiol 1988;69:91–9.

Ge Y, Grossman RI, Babb JS, Rabin ML, Mannon LJ, Kolson DL. Age-related total gray matter and white matter changes in normal adult brain. Part I: volumetric MR imaging analysis. Am J Neuroradiol 2002;23:1327–33.

Giedd JN, Blumenthal J, Jeffries NO, Castellanos FX, Liu H, Zijdenbos A, et al. Brain development during childhood and adolescence: a longitudinal MRI study. Nat Neurosci 1999;2:861–3.

Gonzalez-Burgos G, Kroener S, Zaitsev AV, Povysheva NV, Krimer LS, Barrionuevo G, et al. Functional maturation of excitatory synapses in layer 3 pyramidal neurons during postnatal development of the primate prefrontal cortex. Cereb Cortex 2008;18:626–37.

Gordon E, Cooper NJ, Rennie CJ, Hermens D, Williams LM. Integrative neuroscience: the role of a standardised database. Clin Electroencephalogr Neurosci 2005;36:64–75.

Gratton G, Coles MGH, Donchin E. A new method for off-line removal of ocular artifact. Electroencephalogr Clin Neurophysiol 1983;55:468–84.

Gur RC, Mozley PD, Resnick SM, Gottlieb GL, Kohn M, Zimmerman R, et al. Gender differences in age effect on brain atrophy measured by magnetic resonance imaging. Proc Nat Acad Sci USA 1991;88:2845–9.
Gutiérrez R, Bioson D, Heinemann U, Stoffel W. Decompaction of CNS myelin leads to a reduction of the conduction velocity of action potentials in optic nerve. Neurosci Lett 1995;195:93–6.
Gutiérrez A, Khan ZU, Miralles CP, Mehta AK, Ruano D, Araujo F, et al. $GABA_A$ receptor subunit expression changes in the rat cerebellum and cerebral cortex during aging. Mol Brain Res 1997;45:59–70.
Hartikainen P, Soininen H, Partanen J, Helkala EL, Riekkinen P. Aging and spectral analysis of EEG in normal subjects: a link to memory and CSF AChE. Acta Neurol Scand 1992;86:148–55.
Hatazawa J, Ito M, Yamaura H, Matsuzawa T. Sex differences in brain atrophy during aging: a quantitative study with computed tomography. J Am Geriatr Soc 1982;30:235–9.
Haug H. Brain sizes, surfaces, and neuronal sizes of the cortex cerebri: a stereological investigation of man and his variability and a comparison with some mammals (primates, whales, marsupials, insectivores, and one elephant). Am J Anat 1987;180:126–42.
Heinen K, Baker RE, Spijker S, Rosahl T, van Pelt J, Brussaard AB. Impaired dendritic spine maturation in $GABA_A$ receptor α1 subunit knock out mice. Neuroscience 2003;122:699–705.
Hill AAV, Edwards DH, Murphey RK. The effect of neuronal growth on synaptic integration. J Comp Neurosci 1994;1:239–54.
Hollander M, Wolfe DA. Nonparametric statistical methods. New York: Wiley; 1973.
Hortobágyi T, Fernandez del Olmo M, Rothwell JC. Age reduces cortical reciprocal inhibition in humans. Exp Brain Res 2006;171:322–9.
Hubbard B, Anderson J. Sex differences in age-related brain atrophy. Lancet 1983;321:1446–8.
Hughes J. Normal limits of the EEG. In: Halliday R, Butler S, Paul R, editors. A textbook of clinical neurophysiology. New York: Wiley; 1987. p. 105–54.
Hughes JR, Cayaffa JJ. The EEG in patients at different ages without organic cerebral disease. Electroencephalogr Clin Neurophysiol 1977;42:776–84.
Huttenlocher PR. Morphometric study of human cerebral cortex development. Neuropsychologia 1990;28:517–27.
Jacobs B, Driscoll L, Schall M. Life-span dendritic and spine changes in areas 10 and 18 of human cortex: a quantitative Golgi study. J Comp Neurol 1997;386:661–80.
Jirsa VK, Haken H. Field theory of electromagnetic brain activity. Phys Rev Lett 1996;77:960–3.
Jirsa VK, Haken H. A derivation of a macroscopic field theory of the brain from the quasi-microscopic neural dynamics. Physica D 1997;99:503–26.
John ER, Ahn H, Prichep L, Trepetin M, Brown D, Kaye H. Developmental equations for the electroencephalogram. Science 1980;210:1255–8.
Katz RI, Horowitz GR. Electroencephalogram in the septuagenarian: studies in a normal geriatric population. J Am Geriatr Soc 1982;30:273–5.
Kemper TL. Neuroanatomical and neuropathological changes during aging and dementia. In: Albert ML, Knoefel JE, editors. Clinical neurology of aging. New York: Oxford University Press; 1994.
Kerr CC, Rennie CJ, Robinson PA. Physiology-based modeling of cortical auditory evoked potentials. Biol Cybern 2008;98:171–84.
Kerr CC, Rennie CJ, Robinson PA. Deconvolution analysis of target evoked potentials. J Neurosci Meth 2009;179:101–10.
Kerr CC, van Albada SJ, Rennie CJ, Robinson PA. Age trends in auditory oddball evoked potentials via component scoring and deconvolution. in preparation.
Klimesch W. EEG alpha and theta oscillations reflect cognitive and memory performance: a review and analysis. Brain Res Rev 1999;29:169–95.
Koenderink MJT, Uylings HBM. Postnatal maturation of layer V pyramidal neurons in the human prefrontal cortex. A quantitative Golgi analysis. Brain Res 1995;678:233–43.
Kooi KA. Fundamentals of electroencephalography. New York: Harper & Row; 1971.
Kuhl D, Metter E, Riege W, Phelps M. Effects of human aging on patterns of local cerebral glucose utilization determined by the [18F]fluorodeoxyglucose method. J Cereb Blood Flow Metab 1982;2:163–71.
Lopes da Silva FH, Hoeks A, Smits H, Zetterberg LH. Model of brain rhythmic activity. The alpha rhythm of the thalamus. Kybernetik 1974;15:27–37.
Luebke JI, Rosene DL. Aging alters dendritic morphology, input resistance, and inhibitory signaling in dentate granule cells of the rhesus monkey. J Comp Neurol 2003;460:573–84.
Luebke JI, Chang Y-M, Moore TL, Rosene DL. Normal aging results in decreased synaptic excitation and increased synaptic inhibition of layer 2/3 pyramidal cells in the monkey prefrontal cortex. Neuroscience 2004;125: 277–88.
Magnusson KR, Nelson SE, Young AB. Age-related changes in the protein expression of subunits of the NMDA receptor. Mol Brain Res 2002;99:40–5.
Matoušek M, Volavka J, Roubíček J, Roth Z. EEG frequency analysis related to age in normal adults. Electroencephalogr Clin Neurophysiol 1967;23:162–7.
Matsuura M, Yamamoto K, Fukuzawa H, Okubo Y, Uesugi H, Moriiwa M, et al. Age development and sex differences of various EEG elements in healthy children and adults. Quantification by a computerized wave form recognition method. Electroencephalogr Clin Neurophysiol 1985;60:394–406.
McEntee W, Crook T. Serotonin, memory, and the aging brain. Psychopharmacology 1991;103:143–9.
Miller A, Alston R, Corsellis J. Variation with age in the volumes of grey and white matter in the cerebral hemispheres of man — measurements with an image analyzer. Neuropath Appl Neurobiol 1980;6:119–32.
Mitzdorf U. Current source-density method and application in cat cerebral cortex: investigation of evoked potentials and EEG phenomena. Physiol Rev 1985;65:37–100.
Morrison J, Hof P. Life and death of neurons in the aging brain. Science 1997;278:412–9.
Nelder JA, Mead R. A simplex method for function minimization. Computer J 1965;7:308–13.
Niedermeyer E. Maturation of the EEG: development of waking and sleeping patterns. In: Niedermeyer E, Lopes da Silva F, editors. Electroencephalography, basic principles, clinical applications, and related fields. Baltimore: Urban & Schwarzenberg; 1982. p. 107–30.
Nunez PL. Wave-like properties of the alpha rhythm. IEEE Trans Biomed Eng 1974;21:473–83.
Nunez PL. Neocortical dynamics and human EEG rhythms. New York: Oxford University Press; 1995.
Obrist WD. The electroencephalogram of normal aged adults. Electroencephalogr Clin Neurophysiol 1954;6:235–44.
Olkin I, Finn JD. Correlations redux. Psychol Bull 1995;118:155–64.
Ontl T, Xing Y, Bai L, Kennedy E, Nelson S, Wakeman M, et al. Development and aging of *N*-methyl-D-aspartate receptor expression in the prefrontal/frontal cortex of mice. Neuroscience 2004;123:467–79.
Pakkenberg B, Gundersen HJG. Neocortical neuron number in humans: effect of sex and age. J Comp Neurol 1997;384:312–20.
Pantano P, Baron J-C, Lebrun-Grandié P, Duquesnoy N, Bousser M-G, Comar D. Regional cerebral blood flow and oxygen consumption in human aging. Stroke 1984;15:635–41.
Passe TJ, Rajagopalan P, Tupler LA, Byrum CE, MacFall JR, Krishnan RR. Age and sex effects on brain morphology. Prog Neuro-Psychopharmacol Biol Psychiat 1997;21:1231–7.
Peinemann A, Lehner C, Conrad B, Siebner HR. Age-related decrease in paired-pulse intracortical inhibition in the human primary motor cortex. Neurosci Lett 2001;313:33–6.
Perrin JS, Hervé P-Y, Leonard G, Perron M, Pike GB, Pitiot A, et al. Growth of white matter in the adolescent brain: role of testosterone and androgen receptor. J Neurosci 2008;28:9519–24.
Petanjek Z, Judaš M, Kostović I, Uylings BM. Lifespan alterations of basal dendritic trees of pyramidal neurons in the human prefrontal cortex: a layer-specific pattern. Cereb Cortex 2008;18:915–29.
Peters A. Structural changes that occur during normal aging of primate cerebral hemispheres. Neurosci Biobehav Rev 2002a;26:733–41.
Peters A. The effects of normal aging on myelin and nerve fibers: a review. J Neurocytol 2002b;31:581–93.
Petersén I, Eeg-Olofsson O. The development of the electroencephalogram in normal children from the ages of 1 through 15 years. Neuropädiatrie 1971;2:247–304.
Petersén I, Selldén U, Eeg-Olofsson O. The evolution of the EEG in normal children and adolescents from 1 to 21 years. In: Rémond A, Lairy GC, editors. Handbook of electroencephalography and clinical neurophysiology. Amsterdam: Elsevier; 1975. p. 31–68.
Piguet O, Double KL, Kril JJ, Harasty J, Macdonald V, McRitchie DA, et al. White matter loss in healthy ageing: a postmortem analysis. Neurobiol Aging 2009;30:1288–95.
Poe BH, Linville C, Brunso-Bechtold J. Age-related decline of presumptive inhibitory synapses in the sensorimotor cortex as revealed by the physical disector. J Comp Neurol 2001;439:65–72.
Polich J. EEG and ERP assessment of normal aging. Electroencephalogr Clin Neurophysiol 1997;104:244–56.
Press WH, Teukolsky SA, Vetterling WT, Flannery BP. Numerical recipes in C. 2nd ed. Cambridge: Cambridge University Press; 1992.
R Development Core Team. R: a language and environment for statistical computing. Vienna: R Foundation for Statistical Computing; 2005.
Rapp P, Gallagher M. Preserved neuron number in the hippocampus of aged rats with spatial learning deficits. Proc Nat Acad Sci USA 1996;93:9926–30.
Rasmussen T, Schliemann T, Sørensen J, Zimmer J, West M. Memory impaired aged rats: no loss of principal hippocampal and subicular neurons. Neurobiol Aging 1996;17:143–7.
Ray W. The electrocortical system. In: Cacioppo J, Tassinary LG, editors. Principles of psychophysiology. Cambridge: Cambridge University Press; 1990. p. 385–412.
Rennie CJ, Robinson PA, Wright JJ. Effects of local feedback on dispersion of electrical waves in the cerebral cortex. Phys Rev E 1999;59:3320–9.
Rennie CJ, Wright JJ, Robinson PA. Mechanisms of cortical electrical activity and emergence of gamma rhythm. J Theor Biol 2000;205:17–35.
Rennie CJ, Robinson PA, Wright JJ. Unified neurophysical model of EEG spectra and evoked potentials. Biol Cybern 2002;86:457–71.
Roberts JA, Robinson PA. Modeling absence seizure dynamics: implications for basic mechanisms and measurement of thalamocortical and corticothalamic latencies. J Theor Biol 2008;253:189–201.
Robinson PA. Neurophysical theory of coherence and correlations of electroencephalographic signals. J Theor Biol 2003;222:163–75.
Robinson PA, Rennie CJ, Wright JJ. Propagation and stability of waves of electrical activity in the cerebral cortex. Phys Rev E 1997;56:826–40.
Robinson PA, Rennie CJ, Wright JJ, Bourke PD. Steady states and global dynamics of electrical activity in the cerebral cortex. Phys Rev E 1998;58:3557–71.
Robinson PA, Rennie CJ, Wright JJ, Bahramali H, Gordon E, Rowe DL. Prediction of electroencephalographic spectra from neurophysiology. Phys Rev E 2001a;63:021903.1–021903.18.

Robinson PA, Loxley PN, O'Connor SC, Rennie CJ. Modal analysis of corticothalamic dynamics, electroencephalographic spectra, and evoked potentials. Phys Rev E 2001b;63:041909.1–041909.13.
Robinson PA, Rennie CJ, Rowe DL. Dynamics of large-scale brain activity in normal arousal states and epileptic seizures. Phys Rev E 2002;65:041924.1–4.9.
Robinson PA, Rennie CJ, Rowe DL, O'Connor SC, Wright JJ, Gordon E, et al. Neurophysical modeling of brain dynamics. Neuropsychopharmacology 2003;28(Suppl. 1):74–9.
Robinson PA, Rennie CJ, Rowe DL, O'Connor SC. Estimation of multiscale neurophysiologic parameters by electroencephalographic means. Hum Brain Mapp 2004;23:53–72.
Rossini PM, Rossi S, Babiloni C, Polich J. Clinical neurophysiology of aging brain: from normal aging to neurodegeneration. Prog Neurobiol 2007;83:375–400.
Rowe DL, Robinson PA, Rennie CJ. Estimation of neurophysiological parameters from the waking EEG using a biophysical model of brain dynamics. J Theor Biol 2004;231:413–33.
Salinsky MC, Oken BS, Morehead L. Test–retest reliability in EEG frequency analysis. Electroencephalogr Clin Neurophysiol 1991;79:382–92.
Saunders MG. Artifacts: activity of noncerebral origin in the EEG. In: Klass DW, Daly DD, editors. Current practice of clinical electroencephalography. New York: Raven; 1979. p. 37–67.
Scahill R, Frost C, Jenkins R, Whitwell J, Rossor M, Fox N. A longitudinal study of brain volume changes in normal aging using serial registered magnetic resonance imaging. Arch Neurol 2003;60:989–94.
Schiff SJ, Huang X, Wu J-Y. Dynamical evolution of spatiotemporal patterns in mammalian middle cortex. Phys Rev Lett 2007;98:178102.1–2.4.
Segovia G, Porras A, Del Arco A, Mora F. Glutamatergic neurotransmission in aging: a critical perspective. Mech Ageing Dev 2001;122:1–29.
Shapiro SS, Wilk MB. An analysis of variance test for normality (complete samples). Biometrika 1965;52:591–611.
Simonyi A, Ngomba RT, Storto M, Catania MV, Miller LA, Youngs B, et al. Expression of groups I and II metabotropic glutamate receptors in the rat brain during aging. Brain Res 2005;1043:95–106.
Somsen RJM, van 't Klooster BJ, van der Molen MW, van Leeuwen HMP, Licht R. Growth spurts in brain maturation during middle childhood as indexed by EEG power spectra. Biol Psychol 1997;44:187–209.
Sowell ER, Trauner DA, Gamst A, Jernigan TL. Development of cortical and subcortical brain structures in childhood and adolescence: a structural MRI study. Dev Med Child Neurol 2002;44:4–16.
Sowell ER, Peterson BS, Thompson PM, Welcome SE, Henkenius AL, Toga AW. Mapping cortical change across the human life span. Nat Neurosci 2003;6:309–15.
Sowell ER, Thompson PM, Leonard CM, Welcome SE, Kan E, Toga AW. Longitudinal mapping of cortical thickness and brain growth in normal children. J Neurosci 2004;24:8223–31.
Stam CJ, Pijn JPM, Suffczynski P, Lopes da Silva FH. Dynamics of the human alpha rhythm: evidence for non-linearity? Clin Neurophysiol 1999;110: 1801–13.
Suhara T, Fukuda H, Inoue O, Itoh T, Suzuki K, Yamasaki T, et al. Age-related changes in human D1 dopamine receptors measured by positron emission tomography. Psychopharmacology 1991;103:41–5.
Sullivan EV, Rosenbloom M, Serventi KL, Pfefferbaum A. Effects of age and sex on volumes of the thalamus, pons, and cortex. Neurobiol Aging 2004;25:185–92.
Tennigkeit F, Schwarz DWF, Puil E. Postnatal development of signal generation in auditory thalamic neurons. Dev Brain Res 1998;109:255–63.
Thompson PM, Giedd JN, Woods RP, MacDonald D, Evans AC, Toga AW. Growth patterns in the developing brain detected by using continuum mechanical tensor maps. Nature 2000;404:190–3.
Tomlinson B, Blessed G, Roth M. Observations on the brains of non-demented old people. J Neurol Sci 1968;7:331–56.
Towe AL. On the nature of the primary evoked response. Exp Neurol 1966;15:113–39.
Uylings HBM, de Brabander JM. Neuronal changes in normal human aging and Alzheimer's disease. Brain Cogn 2002;49:268–76.
van Albada SJ, Rennie CJ, Robinson PA. Variability of model-free and model-based quantitative measures of EEG. J Integ Neurosci 2007;6:279–307.
van der Werf YD, Tisserand DJ, Visser PJ, Hofman PAM, Vuurman E, Uylings HBM, et al. Thalamic volume predicts performance on tests of cognitive speed and decreases in healthy aging: a magnetic resonance imaging-based volumetric analysis. Cogn Brain Res 2001;11:377–85.
Veldhuizen RJ, Jonkman EJ, Poortvliet DCJ. Sex differences in age regression parameters of healthy adults — normative data and practical implications. Electroencephalogr Clin Neurophysiol 1993;86:377–84.
Volkow N, Logan J, Fowler J, Wang G-J, Gur R, Wong C, et al. Association between age-related decline in brain dopamine activity and impairment in frontal and cingulate metabolism. Am J Psychiatry 2000;157:75–80.
Warren RA, Jones EG. Maturation of neuronal form and function in a mouse thalamo-cortical circuit. J Neurosci 1997;17:277–95.
Williams LM, Gatt JM, Hatch A, Palmer DM, Nagy M, Rennie CJ, et al. The INTEGRATE Model of emotion, thinking and self regulation: an application to the "Paradox of Aging". J Integ Neurosci 2008;7:367–404.
Wilson HR, Cowan JD. Excitatory and inhibitory interactions in localized populations of model neurons. Biophys J 1972;12:1–24.
Wilson HR, Cowan JD. A mathematical theory of the functional dynamics of cortical and thalamic nervous tissue. Kybernetik 1973;13:55–80.
Wright JJ, Liley DTJ. Simulation of electrocortical waves. Biol Cybern 1995;72:347–56.
Xi M-C, Liu R-H, Engelhardt KK, Morales FR, Chase MH. Changes in the axonal conduction velocity of pyramidal tract neurons in the aged cat. Neuroscience 1999;92:219–25.
Xu J, Kobayashi S, Yamaguchi S, Iijima K, Okada K, Yamashita K. Gender effects on age-related changes in brain structure. Am J Neuroradiol 2000;21:112–8.
Xu W, Huang X, Takagaki K, Wu J-Y. Compression and reflection of visually evoked cortical waves. Neuron 2007;55:119–29.
Zemcov A, Barclay L, Blass J. Regional decline of cerebral blood flow with age in cognitively intact subjects. Neurobiol Aging 1984;5:1–6.